Abnormal expression of splicing regulators RBFOX and NOVA is associated with aberrant splicing patterns at the Neurexin-3 gene in a monogenic autism spectrum disorder

Pedro K. K. Forti[1,2,6], Lilian L. Depieri[1,6], Lucas A. Giorgiani[1,6], Breno B. Hernandes[1,2], João G. Bueno[1], Gustavo D. Verçosa[1,2], Israel C. Vasconcelos[2,3], Mario H. Bengtson[3,4], Marcelo F. Carazzolle[1], Antonio P. Camargo[5], Fabio Papes[1,*]

[1] Department of Genetics, Evolution, Microbiology and Immunology, Institute of Biology, University of Campinas, Campinas, Sao Paulo, 13083-862, Brazil

[2] Graduate Program in Genetics and Molecular Biology, Institute of Biology, University of Campinas, Campinas, Sao Paulo, 13083-862, Brazil

[3] Center for Medicinal Chemistry, University of Campinas, Campinas, Sao Paulo, 13083-875, Brazil

[4] Department of Biochemistry and Tissue Biology, Institute of Biology, University of Campinas, Campinas, Sao Paulo, 13083-862, Brazil

[5] Department of Biochemistry, Institute of Chemistry, University of Sao Paulo, Sao Paulo, 05508-000, Brazil

[6] These authors contributed equally.

*** Corresponding author's contact info:**

Fabio Papes, Ph.D
Department of Genetics, Evolution, Microbiology and Immunology, Institute of Biology,
University of Campinas; Rua Monteiro Lobato, 255, Campinas, SP, 13083-862, Brazil

E-mail address: papesf@unicamp.br

Abstract

Autism spectrum disorders are diseases characterized by a combination of cognitive, behavioral and neurological symptoms. A complex interplay between environmental factors and a multitude of genetic determinants, most of them composed of low-risk variants, impose difficulties in understanding the molecular and cellular underpinnings of these conditions. In some cases, autistic patients have been shown to display alterations in splicing patterns of several genes, but the extent to which this phenomenon is common in the context of these multifactorial disorders is unknown, nor is it known if monogenic cases of autism also display dysregulation of splicing. Moreover, very few studies have investigated the causal links between splicing alterations in specific genes and the phenotypic characteristics of the neural tissue in autism patients. In this study, we have focused on a monogenic type of autism caused by haploinsufficiency of the Transcription Factor 4 gene, known as Pitt-Hopkins Syndrome. We show that neurons and organoids derived from patients with this disease have altered expression of splicing regulators in the NOVA and RBFOX families, accompanied by aberrant splicing patterns in a substantial number of genes involved in neural tissue development and synapse organization. We focused on a gene encoding a member of the Neurexin Family, the splicing of which normally leads to the production of transcript variants coding for both transmembrane and secreted protein isoforms. In Pitt-Hopkins Syndrome neurons, we detected an aberrant splicing pattern that results in lower expression of the secreted isoform and its corresponding transcript, a phenomenon that may explain why the neural tissue in these patients have decreased electrical activity through impaired synapse organization. Our data shed light on the role splicing regulation plays in a monogenic type of autism.

INTRODUCTION

RNA splicing plays a critical role in regulating transcription and producing the wide diversity of transcripts and protein isoforms that characterize the eukaryotic cell. Alternative splicing results in the joining of exons and exclusion of introns in different configurations, being classified as exon skipping (SE), intron retention (RI), alternative 5' or 3' splice site (A5SS or A3SS), and mutually exclusive exon (MXE) splicing events[1]. RNA splicing is tightly regulated by RNA-binding proteins, several of which are important to neurogenesis, axon guidance, synaptogenesis, and synaptic physiology during neurodevelopment[2].

Alternative splicing is very prevalent in the human brain, particularly during neuronal differentiation[3], affecting events such as synaptic function and stability[4]. Aberrant splicing patterns at genes involved in synaptic plasticity such as *NLGN3*, *NLGN4*, *NRXN1*, *SHANK3*, and *CADPS2* are present in individuals with autism-spectrum disorders[5], which has been taken as a suggestion that several of these genes may have a putative role in the molecular mechanisms driving autism.

Out of the many RNA-binding proteins regulating splicing, two families have been linked to autism in several studies – RNA Binding Fox-1 Homolog (RBFOX) and Neuro-Oncological Ventral Antigen (NOVA) proteins. RBFOX family members RBFOX1, RBFOX2, and RBFOX3 are expressed in neurons[6], regulating alternative splicing patterns particularly during early neurogenesis and for synaptic plasticity (RBFOX1 and RBFOX2) or in mature neurons (RBFOX3)[7]. RBFOX1 controls the skipping of neuron-specific exons in many genes, particularly in those related to synapse formation, like *NRCAM* and *GRIN1*, which are dysregulated in samples of autistic children[8]. Likewise, NOVA1 has been shown to bind introns flanking neuron-specific exons, leading to exon inclusion or skipping[9]. In the brains of autistic children or individuals with other types of neurodevelopmental disorders, some studies have identified downregulation of RBFOX and NOVA family members[1,10], and several direct RBFOX and NOVA target genes are involved in synaptic transmission or ion channel regulation[1,11]. Additionally, RBFOX variants have been associated with several conditions characterized by neuropsychiatric symptoms[12].

Despite recent advances in understanding the role played by the dysregulation of RNA splicing regulators in the pathogenesis of autism, little is known about how mutations in specific genes causing autism-spectrum disorders lead to RBFOX and NOVA alterations and aberrant splicing patterns in downstream genes. This gap of knowledge prompted us to investigate a

monogenic type of autism. Here, we have studied the occurrence of aberrant alternative splicing patterns in a monogenic autism disease called Pitt-Hopkins Syndrome (PTHS; MIM 610954)[13–16]. PTHS is caused by de novo heterozygous mutations in the Transcription Factor 4 gene (*TCF4*; OMIM 602272), which encodes a bHLH transcription factor expressed in the brain[17–20] and important for neurodevelopment, neural lineage commitment, and neuronal physiology[21–26]. PTHS individuals exhibit severe cognitive deficit, motor delay, hypotonia, respiratory abnormalities, autistic behaviors, chronic constipation, and distinctive facial features[27,28]. Interestingly, variants of the *TCF4* gene have also been associated with schizophrenia, bipolar disorder, post-traumatic stress disorder, and major depressive disorder[29–33], suggesting that part of the underlying molecular mechanisms may be common between these conditions and autism. Our choice to study aberrant splicing in PTHS is due to its monogenetic nature, which allows us to dissect its pathological molecular mechanisms and more precisely correlate them with the cellular abnormalities found in the PTHS neural tissue.

We have previously generated and analyzed neural progenitor cells, neurons, and brain organoids from patients with PTHS to analyze the molecular phenotypes of the diseased neural tissue[34,35]. We showed that PTHS neural progenitors cultured using traditional 2D techniques and neural progenitors in PTHS organoids display a deficit in proliferation and severely diminished differentiation rate into neurons. Strikingly, we detected that PTHS organoids representative of the cerebral cortex are aberrant in size and structure, containing a higher percentage of neural progenitor cells and fewer cortical neurons of many subtypes, including deep-layer and superficial-layer excitatory neurons; moreover, PTHS organoids representative of the subpallial region exhibit a deficient content of cortical-type GABAergic interneurons[34]. Importantly, PTHS neurons in 2D culture and the neural network of PTHS organoids are characterized by severely impaired electrical activity, as judged by patch-clamp and multi-electrode array assays, respectively. Additionally, assessment of neuronal activity via FOS expression revealed that FOS+ neurons are fewer in PTHS organoids, concomitant with a lower expression of excitatory neuron's synaptic markers vGLUT1 and vGLUT2[34], suggesting that synapse formation is altered in this type of autism.

In this paper, we studied the expression of RBFOX and NOVA splicing regulators in PTHS neurons, showing that the lower expression of those regulators is accompanied by distinct splicing profiles in a range of genes, in comparison with neurons of normal genotype. These aberrant splicing patterns affect several genes coding for proteins important for synapse physiology, including Neurexin genes. We found that the Neurexin-3 gene (*NRNX3*) displays an

aberrant pattern of splicing involving an exon skipping event, where PTHS neurons have relatively lower abundance of a transcript variant that includes an exon leading to a premature stop codon and producing a soluble secreted form of Neurexin. On the other hand, neurons from donors of normal genotype exhibit lower abundance of the other transcript variant (excluding the exon), which produces a transmembrane Neurexin thought to be involved in synapse formation and stability[36]. Our findings show the novel information that a severe form of autism is accompanied by altered splicing of a gene encoding a synaptic component, leading to an imbalance between different Neurexin neuronal isoforms, which may contribute to the PTHS neural tissue's impaired electrical activity.

121 ## RESULTS

122 **Altered expression of splicing regulators *RBFOX1/2/3* and *NOVA1* in Pitt-Hopkins**
123 **Syndrome neurons in 2D culture**

124 We have previously shown that the neural tissue in Pitt-Hopkins Syndrome (PTHS) is
125 characterized by poor proliferation of neural progenitor cells and impaired differentiation of
126 cortical neurons, in both traditional 2D neuronal cultures and in patient-derived cortical
127 organoids[34]. We also detected lower neural activity in PTHS neurons, which could be in part due
128 to impaired synaptogenesis. Importantly, we analyzed the gene expression profiles of both
129 PTHS neurons and organoids via bulk RNA sequencing followed by differential gene expression
130 analysis[34] to identify dysregulated genes and pathways that could potentially be causally
131 implicated with these phenotypes. These transcriptomic data were obtained from 4 PTHS
132 patients harboring heterozygous mutations in the *TCF4* gene, causally related to the disease[34].

133 Interestingly, we noticed that several entries in the list of differentially expressed genes between
134 PTHS samples and same-sex parental controls code for RNA splicing regulators, such as RNA
135 Binding Fox-1 Homolog 1 (RBFOX1), RBFOX2, and RBFOX3, as well as Neuro-Oncological
136 Ventral Antigen 1 (NOVA1) and NOVA2 (Supplementary Table S1)[34]. Even though *NOVA2* is
137 also downregulated in PTHS neurons in 2D culture, its overall expression levels across parental
138 controls and patients are lower than *NOVA1* (Supplementary Table S1). Therefore, we decided
139 to focus our efforts on understanding the role played by *NOVA1* and *RBFOX1/2/3* in triggering
140 aberrant splicing patterns in PTHS.

141 In fact, several patient-parent pairs exhibited lower expression of *RBFOX1/2/3* and *NOVA1*
142 genes in PTHS neurons. For *RBFOX1*, the fold-changes (in log base 2) of expression in the
143 comparison between patient-control pairs #1, #2, and #3 are -4.95, -2.03, and -5.1, respectively
144 (Fig. 1a-d); for patient #4, the expression is low, comparable to the levels displayed by the other
145 3 patients, although a matching parental control was unavailable in this case (Supplementary
146 Table S1). For *RBFOX2*, the fold-changes between patient-control pairs #1, #2, and #3 are -
147 2,26, -1.79, and -1,61, respectively (Fig. 1a-d and Supplementary Table S1). *RBFOX3,* the most
148 studied splicing regulator in neurons, coding for the neuronal marker NeuN, exhibits fold-
149 changes of -10.9, -2,93, and -5,14, for pairs #1, #2, and #3, respectively (Fig. 1a-d and
150 Supplementary Table S1). Finally, *NOVA1* is also significantly less expressed in PTHS samples
151 as compared to parental controls for patient-control pairs #1, #2, and #3 (Fig. 1a-d), and its
152 expression is low in patient #4 (Supplementary Table S1).

153 The impaired expression of *RBFOX1/2/3* and *NOVA1* in PTHS neurons seems to be specific to
154 this neural cell category, as PTHS neural progenitor cells do not show a diminishment in the
155 expression levels of such genes: only the expression of *RBFOX1* is lower in patient-parent pairs
156 #1 to #4, while the other genes show average fold-changes close to zero (Fig. 1e-i). Importantly,
157 the overall expression abundance of these genes is somewhat lower in neural progenitor cells
158 as compared to neurons, as judged by the metric of expression abundance TPM (transcripts per
159 million reads) (Supplementary Table S1).

160 Next, we performed independent neuronal differentiation experiments to quantify the expression
161 of *NOVA1* and *RBFOX1/2/3* in PTHS neurons via reverse transcriptase-coupled quantitative
162 PCR (RT-qPCR) in comparison with two controls of normal genotype. Similar to the
163 transcriptomic data obtained from bulk RNA-Seq experiments in 2D cultured neurons, *RBFOX1*
164 expression levels were -1.9, -1.5, and -0.9-fold lower in patients #1, #2, and #3 in the
165 comparison with control #1, or -1.8, -1.5, and -0.8-fold lower in patients #1, #2, and #3 in the
166 comparison with control #3 (Fig. 1j). Similarly, *RBFOX2* expression levels were also lower in
167 patients #1, #2, and #3 in the comparison with control #1 and in patient #2 in the comparison
168 with control #3 (Fig. 1j). On the other hand, *RBFOX3* expression was only found to be lower in
169 patient #2, and NOVA1 expression was lower in patients #1 and #2 in the comparison with
170 patient #1 (Fig. 1j).

171 In combination, the RNA-Seq and qPCR results indicate that splicing regulators in the NOVA
172 and RBFOX families have lower expression levels in neurons of certain PTHS individuals
173 cultured using traditional 2D techniques. It is noteworthy that *RBFOX1* is consistently
174 downregulated in PTHS neurons across all subjects in our cohort.

175

176 **Complex dysregulation in the expression of *RBFOX1/2/3* and *NOVA1* in Pitt-Hopkins**
177 **Syndrome cortical and subpallial organoids**

178 Because there was a difference in expression abundances for *RBFOX1/2/3* and *NOVA1*
179 between two different neural cell types in our bulk RNA-Seq data, we sought to explore the
180 expression of these genes in single-cell transcriptomic data from PTHS patient-derived cortical
181 and subpallial organoids, which are complex 3D structures able to model the events that
182 happen during early neurodevelopment in vivo and. These models are more representative of
183 the molecular characteristics of neuronal cells than traditional 2D cultures[34,37,38]. Because the
184 organoids contain a more diverse set of neurons and the interactions between different cell

185 types may influence the dysregulation of *NOVA* and *RBFOX* expression, we reasoned that the
186 organoids would more faithfully recapitulate the changes in expression occurring in vivo. In
187 organoid single-cell RNA sequencing (scRNA-Seq) libraries previously described by our
188 group[34], we could annotate six neural cell subpopulations, including progenitor cells,
189 intermediate progenitors, and neurons[34] in two distinct differentiation lineages that produce
190 either glutamatergic or GABAergic neurons (Fig. 2a). In cortical organoids (CtOs), the
191 predominant differentiation lineage leads to glutamatergic neurons (Fig. 2b), while subpallial
192 organoids (sPOs) generate mostly GABAergic cells (Fig. 2b), matching the differentiation profile
193 found in the cortex and subpallial brain regions in vivo[39,40].

194 The fractions of cells expressing *NOVA1* are substantial in control CtO and sPO subpopulations
195 (Fig. 2c,d) – 80.3% of CtO progenitor cells (Pr-Glut), 67.6% of CtO intermediate progenitor cells
196 (IP-Glut), 49.1% of CtO glutamatergic neurons (N-Glut), 96.2% of sPO progenitor cells (Pr-
197 GABA), 97.1% of sPO intermediate progenitor cells (IP-GABA), and 98.4% of sPO GABAergic
198 neurons (N-GABA) express *NOVA1* above a threshold level of 0.5. Curiously, *NOVA1*
199 expression remains stable along the differentiation trajectory from progenitor cells to neurons in
200 the glutamatergic lineage of control CtOs (Fig. 2c) (mean expression of 1.77, 1.26, and 1.3 in
201 Pr-Glut, IP-Glut, and N-Glut, respectively), whereas expression increases from progenitors to
202 neurons in the GABAergic lineage of control sPOs (Fig. 2d) (mean expression of 5.7, 5.6, and
203 12.0 in Pr-GABA, IP-GABA, and N-GABA, respectively).

204 In contrast, the numbers of cells expressing *RBFOX1* are much lower than those expressing
205 *NOVA1,* across all CtO and sPO subpopulations (Fig. 2e,f) – 1.56% of CtO progenitor cells (Pr-
206 Glut), 3.21% of CtO intermediate progenitor cells (IP-Glut), 10.7% of CtO glutamatergic neurons
207 (N-Glut), 0.6% of sPO progenitor cells (Pr-GABA), 2.0% of sPO intermediate progenitor cells
208 (IP-GABA), and 8.8% of sPO GABAergic neurons (N-GABA) express *RBFOX1* above a
209 threshold level of 0.5. *RBFOX1* expression increases dramatically along the differentiation
210 trajectory from progenitor cells to neurons in both the glutamatergic and GABAergic lineages of
211 control CtOs and sPOs, respectively (Fig. 2e,f) (mean expression of 0.04, 0.06, 0.23, 0.001,
212 0.03, and 0.2 in Pr-Glut, IP-Glut, N-Glut, Pr-GABA, IP-GABA, and N-GABA, respectively).

213 On the other hand, *RBFOX2* is expressed in a large fraction of cells in CtO and sPO
214 subpopulations (Fig. 2g,h) – 55.4% of CtO progenitor cells (Pr-Glut), 84.9% of CtO intermediate
215 progenitor cells (IP-Glut), 73.6% of CtO glutamatergic neurons (N-Glut), 28.9% of sPO
216 progenitor cells (Pr-GABA), 50.3% of sPO intermediate progenitor cells (IP-GABA), and 88.5%
217 of sPO GABAergic neurons (N-GABA) express *RBFOX2* above a threshold level of 0.5. It is

218 very clear that *RBFOX2* expression increases markedly along the differentiation trajectory from
219 progenitor cells to neurons in both the glutamatergic lineage of control CtOs (Fig. 2g) (mean
220 expression of 0.98, 2.1, and 2.6 in Pr-Glut, IP-Glut, and N-Glut, respectively) and the
221 GABAergic lineage of control sPOs (Fig. 2h) (mean expression of 0.46, 0.96, and 3.39 in Pr-
222 GABA, IP-GABA, and N-GABA, respectively).

223 Although *RBFOX3* is a widely recognized neuronal marker, it is expressed in a significant
224 fraction of progenitor cells and intermediate progenitors in CtO and sPO subpopulations (Fig.
225 2i,j) – 11.7% of CtO progenitor cells (Pr-Glut), 49.4% of CtO intermediate progenitor cells (IP-
226 Glut), and 28.5% of CtO glutamatergic neurons (N-Glut), whereas the fractions of sPO cells
227 expressing *RBFOX3* are less prominent – 0% of sPO progenitor cells (Pr-GABA), 4.4% of sPO
228 intermediate progenitor cells (IP-GABA), and 14% of sPO GABAergic neurons (N-GABA)
229 express *RBFOX2* above a threshold level of 0.5. Different than *RBFOX1* and *RBFOX2*,
230 *RBFOX3* expression peaks at the intermediate progenitor stage in the glutamatergic lineage of
231 control CtOs (Fig. 2i) (mean expression of 0.21, 1.0, and 0.53 in Pr-Glut, IP-Glut, and N-Glut,
232 respectively) and increases marginally along the GABAergic lineage of control sPOs (Fig. 2j)
233 (mean expression of 0.007, 0.08, and 0.25 in Pr-GABA, IP-GABA, and N-GABA, respectively).

234 In the comparison between PTHS and control organoids, we verified that the percentage of N-
235 Glut neurons expressing *NOVA1* is higher in PTHS CtOs in contrast to control organoids (left
236 panels in Fig. 3a) and that the percentage of *NOVA1*+ N-GABA neurons remains practically
237 unchanged in PTHS sPOs (right panels in Fig. 3a). Although the mean levels of *NOVA1*
238 expression are statistically significantly different in the comparison between PTHS and control
239 N-Glut neurons in CtOs, being higher in the patient-derived organoids, the effect size is not
240 large (2.0 expression abundance in PTHS versus 1.3 in control; Fig. 2c). Likewise, *NOVA1*
241 expression is statistically significantly higher in PTHS N-GABA neurons of sPOs, and the effect
242 size is similarly not large (14.8 expression abundance in PTHS versus 12.0 in controls; Fig. 2d).

243 Similar to *NOVA1*, the percentages of N-Glut neurons expressing *RBFOX1* and *RBFOX2* are
244 practically unchanged in PTHS CtOs in contrast to control organoids (left panels in Fig. 3b,c),
245 the percentage of N-GABA neurons expressing *RBFOX1* is slightly higher in PTHS sPOs, and
246 the percentage of N-GABA neurons expressing *RBFOX2* is lower in PTHS sPOs (right panels in
247 Fig. 3b,c). Interestingly, the percentages of cells expressing RBFOX3 are higher in both CtOs
248 and sPOs (Fig. 3d). Finally, the mean expression levels of *RBFOX1*, *RBFOX2*, or *RBFOX3* are
249 statistically significantly dysregulated in PTHS N-Glut neurons in CtOs, with small effect sizes
250 (0.19, 3.14, and 1.0 expression abundances in PTHS versus 0.23, 2.6, and 0.53 in control,

251 respectively; Fig. 2e,g,i), being higher in PTHS N-GABA neurons of sPOs, with equally small
252 effect sizes (0.74, 3.6, and 0.61 expression abundances in PTHS versus 0.2, 3.4, and 0.25 in
253 control, respectively; Fig. 2f,h,j).

254 The higher expression of *NOVA1* in PTHS CtO and sPO organoids (Fig. 2c,d) as well the higher
255 expression of *RBFOX1/2/3* in PTHS sPO organoids (Fig. 2f,h,j) contrasts with their lower
256 expression in PTHS neurons grown in traditional 2D culture (Fig. 1d). As stated above, this
257 difference may be due to the much wider diversity of cell types and connectivity found in the
258 organoids. Regardless, the bulk and single-cell RNA-Seq results described here and in the
259 previous section indicate alterations in the expression of *NOVA1* and *RBFOX1/2/3* splicing
260 regulators in Pitt-Hopkins Syndrome. These findings prompted us to further investigate possible
261 changes in the RNA splicing process in the patient-derived neural tissue.

262

263 **Aberrant splicing patterns in neurons derived from Pitt-Hopkins Syndrome patients**

264 The consistent finding of altered expression of RBFOX and NOVA splicing regulators in
265 neuronal cultures derived from PTHS patients led us to hypothesize that such dysregulated
266 expression may have led to aberrant splicing. To investigate this, we conducted a computational
267 analysis of the RNA-Seq data from neuronal cultures derived from 5 patient-control pairs using
268 the software rMATS-turbo[41], a computational tool for analyzing alternative splicing using short-
269 read RNA-seq data. In short, rMATS-turbo works by initially using fastq input files to produce
270 splicing graphs for each RNA-seq sample, followed by integration across samples and
271 replicates to quantify alternative splicing events of five basic types: skipped exon (SE),
272 alternative 5′ splice sites (A5SS), alternative 3′ splice sites (A3SS), mutually exclusive exons
273 (MXE) and retained intron (RI). rMATS-turbo adopts the widely used PSI metric to quantify
274 splicing, which represents the percentage of transcripts that include a specific exon or splice
275 site, as calculated from the read counts supporting those specific exons or splice junctions,
276 normalized by the effective lengths of the gene's transcripts[41]. Differences between PSI values
277 in the control and PTHS samples were then computed as ΔPSI, which can be used to infer the
278 existence of different splicing patterns in one or another condition (for example, in PTHS
279 neurons). Positive ΔPSI values imply that the splicing event under analysis is more prevalent in
280 the control samples, while negative ΔPSI values indicate stronger usage in the PTHS samples.

281 After filtering for PSI values (averaged across biological replicates for PTHS or control
282 conditions) smaller than 5% or greater than 95% in both samples, for a false discovery rate

283 smaller than 5% and for |ΔPSI| greater than 5%, we could detect a significant number of splicing
284 events with different PSI in the comparison between neurons derived from each PTHS patient
285 against respective control, in all five categories of splicing (Supplementary Files 1-25). As an
286 example, we could detect 3695 alternative SE events, where one exon of a gene is excluded
287 from a transcript at a higher rate in one sample versus the other, with |ΔPSI| greater than 5% in
288 the comparison between patient and parent #2 (Fig. 4a; Supplementary Table S2). These
289 events were related to transcripts from 2137 different genes (Supplementary Table S2). The
290 numbers of differential splicing events and the numbers of genes in which these events happen,
291 in the 5 patient-control pairs, can be found in Supplementary Table S2. It should be noted that
292 SE events are more numerous than the other types, and RI or A5SS events are the rarest (Fig.
293 4a). When we intersected the splicing events across the five patient-control pairs, we found 492
294 SE events that are common to all pairs (Fig. 4b), in 365 genes (Fig. 4c; Supplementary Table
295 S3). The numbers of common splicing events of the other 4 types are found in Fig. 4b,c and
296 Supplementary Table S3.

297 To better understand the scope of changes in PTHS neurons due to aberrant splicing patterns,
298 we conducted Over-Representation Analysis (ORA) followed by Gene Ontology (GO) and
299 KEGG Pathway analyses, using a list of unique genes for which rMATS-turbo detected splicing
300 events in the comparison between each PTHS patient and a control neuronal cell line. This
301 analysis was performed using the web-based WebGestalt tool[42], which results in an over-
302 representation *z*-score and enrichment *p*-value for each GO term. Interestingly, for SE events,
303 when we analyzed the set of genes from the comparison between patient #2 and its control, we
304 detected a significant enrichment of genes in Gene Ontology-Biological Processes (GO-BP) and
305 KEGG-Pathway categories linked to synapse physiology, axon projection, and cell adhesion
306 (Fig. 4d,e; Supplementary Fig. S1). GO and Pathway analyses results for other patient-control
307 pairs yielded similar results (Supplementary Figure S1), highlighting the possibly relevant role of
308 aberrant splicing patterns in the neural tissue cellular and molecular abnormalities that
309 accompany PTHS.

310 Likewise, we conducted Gene Set Enrichment Analysis (GSEA) followed by Gene Ontology
311 (GO) and KEGG Pathway analyses, using the same list of unique genes for which rMATS-turbo
312 detected splicing events in the comparison between each PTHS patient and a control neuronal
313 cell line. For these analyses, the list of genes was ordered according to the |ΔPSI| values of the
314 corresponding splicing events from rMATS-turbo. GSEA results indicate that, among the genes
315 at the top of the list (meaning genes with splicing events that are more dissimilarly frequent in

316 the comparison between PTHS and control), there are genes related to synapse formation,
317 synapse physiology, and ion transport (Fig. 4f,g; Supplementary Fig. S2). It is interesting to note
318 that the GO and Pathway enrichment analyses described above show the presence of aberrant
319 splicing patterns in genes related to synapse formation, which may be responsible for the lower
320 electrical activity found in PTHS organoids[34].

321 The finding of a substantial number of splicing events that seem to occur differentially between
322 PTHS and control neuronal cell lines led us to hypothesize that the alterations found in the
323 expression levels of *NOVA1* and *RBFOX1/2/3* in PTHS neurons are causally related to the
324 aberrant splicing patterns observed.

325

326 **NOVA1 and RBFOX1/2/3 RNA binding sites are enriched in transcripts predicted to have**
327 **aberrant alternative splicing patterns in PTHS**

328 To further study the relationship between the aberrant splicing patterns observed in PTHS
329 neurons and the dysregulation of expression of NOVA and RBFOX splicing regulators, we
330 investigated the occurrence of NOVA1 and RBFOX1/2/3 binding sites in the genes detected by
331 rMATS-turbo described in the previous section. First, we extracted the genomic sequences
332 containing the exons involved in the SE splicing events detected by rMATS-turbo, plus
333 additional sequences of 200 bp in the neighboring introns. The resulting collection of exon
334 sequences flanked by adjacent introns was then analyzed for RBP (RNA binding protein)
335 binding site enrichment using the SEA program in the MEME suite[43]. Our reasoning was that, if
336 NOVA1 or RBFOX regulators were involved in the aberrant splicing patterns observed in PTHS,
337 then we would expect to see an enrichment in binding sites near the splicing events relative to
338 the occurrence of RBP binding sites in a random collection of genomic sequences. Two NOVA1
339 recognition motifs were analyzed[44] and both were found to be significantly enriched in the
340 genomic sequences near the SE events detected by rMATS-turbo (*E*-values of 9.2×10^{-8} and
341 3.0×10^{-8}; Fisher's exact test; Fig. 5a), with a lower *E*-value than those calculated for a set of
342 genes known to be regulated by NOVA1 (positive control; *E*-values of 2.9×10^{-1} and 1.6×10^{-6},
343 respectively; Fig. 5a; Supplementary File S4). The same type of analysis was conducted for
344 binding site motifs recognized by RBFOX1 and RBFOX2/3 splicing regulators[44], indicating that
345 both are significantly enriched in the genomic sequences near the SE events detected by
346 rMATS-turbo (*E*-values of 5.8×10^{-4} and 4.1×10^{-7}, respectively; Fisher's exact test; Fig. 5a);
347 although these values are larger than those calculated for a set of genes known to be regulated

348 by RBFOX1/2/3 (positive control; *E*-values of 8.4×10^{-8} and 9.2×10^{-16}, respectively; Fig. 5a;
349 Supplementary File S4), the *E*-values are still much smaller than when the enrichment analysis
350 was performed by comparing two randomly chosen sets of genomic sequences (Fig. 5a).

351 Next, we conducted an experiment to detect putative RBP binding sites across the entire
352 genomic sequence of the genes whose splicing patterns were found to be dysregulated by
353 rMATS-turbo. This analysis was performed using the RNA-binding protein motif detection
354 software FIMO in the MEME suite[45]. Examples of genes shown to have enrichment of NOVA1
355 and RBFOX1/2/3 sites are shown in Fig. 5b,c, in comparison with the lower abundance of
356 binding motifs in genes in the random set (negative control; Fig. 5d). We observed a difference
357 in site count which is statistically significant for NOVA1 (Fig. 5e) when considering the genes for
358 the top splicing pattern alterations, as measured by the absolute value of ΔPSI (larger than
359 30%).

360 These enrichment analyses suggest that NOVA1 and RBFOX splicing regulators may be
361 involved in dictating the aberrant splicing patterns observed in PTHS neurons. Direct evidence
362 for this relationship was further pursued by the analysis of published CLiP-Seq (HITS-CLiP)
363 experimental datasets, from studies that performed transcriptome-wide determination of NOVA
364 and RBFOX binding sites[1,11,46]. Considering the 1634 genes harboring aberrant SE splicing
365 events with absolute ΔPSI values larger than 0.1 (larger splicing usage either in the parent or
366 the patient), there is a substantial overlap with the hundreds of genes whose transcripts were
367 shown to be directly bound to NOVA1 (Fig. 5f,g; Supplementary File S5), including genes
368 coding for synapse organization and neuronal physiology. Likewise, there is a very substantial
369 overlap with the thousands of genes whose transcripts have been shown to be directly bound to
370 RBFOX1/2/3 splicing regulators (Fig. 5h; Supplementary File S5).

371 In combination, these results suggest that the altered splicing patterns detected in the
372 transcriptomes of PTHS neurons may be caused by the dysregulation of NOVA1 and
373 RBFOX1/2/3 splicing regulators.

374

375 **The Neurexin-3 gene (*NRXN3*) exhibits an exon skipping event that leads to a transcript**
376 **encoding a soluble protein isoform**

377 Considering that the list of skipped exon (SE) splicing events detected by rMATS-turbo is longer
378 than the lists for the other types of differential splicing events (Fig. 4a), we decided to further

379 investigate this category to better understand the types of events and genes affected by
380 aberrant splicing patterns. GO and Pathway analyses conducted on the list of genes for which
381 rMATS-turbo detected splicing events revealed the presence of genes in enriched categories
382 related to synapse formation and physiology, axonal projection, and cell adhesion (Fig. 4d-g).
383 Curiously, we detected a significant number of splicing events that occur in genes in the
384 Neurexin family, which are traditionally regarded as critical components of synapse
385 physiology[47].

386 In the list of SE splicing events in the comparison between patient-control pairs #1, #2, and #3,
387 we could detect 6, 12, and 1 events, respectively, in genes in the Neurexin family (*NRXN1,*
388 *NRXN2,* and *NRXN3*) (Supplementary File S2). Because some qPCR experiments described
389 below were conducted comparing patient #2 with the parent #1 control (due to non-availability of
390 parent #2 samples), we also conducted the parent #1/patient #2 comparison using rMATS-
391 turbo, which yielded 9 differential SE events linked to *NRXN1/2/3* genes. Finally, in the
392 comparison between parent #2 and patient #4, for whom there is no associated parent in our
393 cohort, we could also detect 2 SE events linked to *NRXN2* and *NRXN3* genes (Supplementary
394 File S2).

395 The numerous events related to *NRXN* genes are further highlighted by the presence of 2
396 events associated with *NRNX2* and *NRXN3* among the top 20 SE splicing events with positive
397 ΔPSI (higher usage in control samples) in the patient #2-parent #2 comparison (Supplementary
398 File S2). The event in the *NRXN2* gene has a ΔPSI equal to 0.681 (Fig. 6a,b), with a higher
399 splicing event usage (ranging from 0.797 to 0.86) in the parent #2 biological replicate libraries,
400 while the PSI values range from 0.117 to 0.196 in the patient #2 samples (Supplementary File
401 S2). It is interesting to note that the exon preferentially included in the transcripts of the *NRXN2*
402 gene in the control sample (SE-NRXN2-i splicing event) is very short (24 nt; Fig. 6b,e) and is
403 equivalent to exon 7 in the *NRXN2* Ensembl transcript ENST00000409571.6. In the PTHS
404 patient, exon 7 is preferentially excluded (SE-NRXN2-e splicing event (Fig. 6b). Interestingly,
405 there exists a 45-bp annotated exon in the same genomic region for the canonical *NRNX2*
406 Ensembl transcript (accession ENST00000265459.11) (Fig. 6c). The only difference between
407 these two annotated transcripts is the 21-bp difference in this exon. The exon skipping event
408 does not lead to a change in the coding sequence reading frame and results in a loss of a few
409 amino acid residues relative to the protein encoded by the canonical transcript (Fig. 6c);
410 therefore, we decided not to pursue this splicing event further.

411 On the other hand, the SE event in the *NRXN3* gene has a ΔPSI equal to 0.608 (Fig. 6d,e), with
412 splicing event inclusion levels ranging from 0.579 to 1.00 in the parent #2 biological replicate
413 libraries, while the PSI values range from 0.167 to 0.185 in patient #2 samples (Supplementary
414 File S2). For ease of reference, we will name the SE event that includes the exon as SE-
415 NRXN3-i, while the splicing configuration that does not include the exon will be called SE-
416 NRXN3-e. Moreover, we chose to call the included exon as E20.5, thus named because it is
417 included between exons 20 and 21 of the canonical *NRXN3* Ensembl transcript
418 ENST00000335750.7 (this exon is also equivalent to exon 19 in the *NRXN3* Ensembl transcript
419 ENST00000554738.5). The exon that is preferentially included in the control samples has a size
420 of 679 nt (Fig. 6e,f). This sequence is found in only 2 out of 14 *NRNX3* Ensembl transcripts with
421 recognized coding sequences (ENST00000554738.5 and ENST00000555387.1); on the other
422 hand, this is not an annotated exon in the canonical *NRXN3* Ensembl transcript
423 (ENST00000335750.7) (Fig. 6f). Additionally, this included exon has been described before in
424 the context of *NRXN3* transcripts expressed in post-mortem human cerebral cortex samples of
425 individuals harboring a SNP near a splicing site in the *NRXN3* gene (rs8019381)[48]. As will be
426 described in detail below, this included exon creates a premature stop codon and the resulting
427 protein truncating transcript variant (PTV) leads to a significantly shorter NRNX3 protein
428 isoform.

429 Interestingly, when we analyzed the sequences of *NRXN2* and *NRXN3* genes using the RNA
430 binding protein binding site motif detection software FIMO[45] (MEME suite), we could detect 4
431 and 223 NOVA1 binding sites in *NRXN2* and *NRNX3* (Fig. 6g,h), respectively. Of these, 1 site
432 falls into adjacent introns and none falls inside the skipped exon for the *NRXN2* event (Fig. 6g),
433 whereas 9 sites fall inside the flanking introns and none falls in the skipped exon for the *NRXN3*
434 splicing event (Fig. 6h). Likewise, we could detect 13 and 156 RBFOX1/2/3 binding sites in the
435 *NRXN2* and *NRNX3* genes (Fig. 6g,h), respectively. Of these, none falls into neighboring introns
436 or inside the skipped exon for the *NRXN2* event (Fig. 6g), while one falls inside the flanking
437 introns and none falls inside the skipped exon for the *NRXN3* splicing event (Fig. 6h).

438 In combination, these results argue in favor of the *NRNX2* and *NRXN3* events under analysis
439 are controlled by NOVA and RBFOX splicing regulators. To confirm the differential splicing in
440 the *NRXN3* gene that creates the SE events mentioned in the previous paragraphs, we decided
441 to conduct reverse-transcription-coupled real-time quantitative PCR (RT-qPCR) as well as
442 standard PCR amplification, using gene-specific primers able to discriminate between those
443 splicing events. To detect the SE-NRXN3-i variant, we placed the forward oligo (p5) in exon 19

444 of the canonical transcript and the reverse oligo (p4) in the splice junction between exons 20
445 and 20.5 (Fig. 7a, right panel). To detect the SE-NRNX3-e variant, we used another forward
446 oligo (p1) in exon 19, and the reverse oligo (p3) was placed in the splice junction between
447 exons 20 and 21 of the canonical *NRXN3* Ensembl transcript ENST00000335750.7. To detect
448 both variants (and the vast majority of transcripts, according to the *NRXN3* Ensembl entry), we
449 used forward and reverse oligos (p1 and p2) in exons 19 and 20, respectively (Fig. 7a, left
450 panel).

451 The mean overall levels of *NRXN3* expression are lower in PTHS individuals, as judged by
452 qPCR with the oligos to globally detect the gene's transcripts (Fig. 7b), which is in keeping with
453 the lower transcriptomic expression found in samples from two PTHS subjects in RNA
454 sequencing experiments (Fig. 7c)[34]. Additionally, the combinations of oligos to detect the SE-
455 NRXN3-i and SE-NRXN3-e splicing variants showed that both have lower expression in PTHS
456 samples (Fig. 7d). Importantly, we calculated the ratio between the expression abundances
457 detected via qPCR for the SE-NRXN3-i versus the SE-NRXN3-e events; compared with the
458 ratios found in patients #1 and #2, controls #1 and #3 have a higher ratio, indicating that the SE-
459 NRXN3-i event is proportionally more abundant than the SE-NRXN3-e event in the control
460 samples in the comparison with the ratio found in those PTHS patient neurons (Fig. 7e).
461 Likewise, these numbers allow us to conclude that the difference in abundances for NRXN3-i
462 and SE-NRXN3-e events is less prominent in patients #1 and #2 than in parents #1 and #3.
463 Curiously, patient #3 also presents an imbalance between both variants, in this case in the
464 opposite direction, which also represents an aberrant splicing pattern with potential functional
465 consequences.

466 To further investigate the SE-NRXN3-i and SE-NRXN3-e splicing events, we used oligos for
467 regular PCR amplification, designed to discriminate between variants based on amplicon size.
468 One pair of primers was placed in exons 20 and 21 (Fig. 7f, top panel); the expected band size
469 for the PCR performed on the SE-NRXN3-e event with this primer pair (p6 and p7) is 334 bp
470 (Fig. 7f), although we could rule out the possibility that other band sizes would exist for other
471 configurations of spliced sites involving exons 20 and 21. Another primer pair (p6 and p8) was
472 placed in exons 20 and 20.5, which is expected to lead to band of size 252 bp only from the SE-
473 NRXN3-i event (Fig. 7f, bottom panel). The PCR results confirm the expected amplicons for
474 these primer pair/splicing event combinations (Fig. 7g), providing experimental evidence that
475 confirms the in silico analyses executed by rMATS-turbo on our PTHS neuron RNA-Seq data,
476 which predicted the existence of the SE-NRXN3-i and SE-NRXN3-e splicing variants.

477 The PCR results showed that we could amplify most of the expected bands that would support
478 the existence of alternative splicing of exon 20.5. However, other bands were also amplified
479 (Fig. 7g), therefore, we decided to clone the amplicons in bulk in a PCR cloning vector, followed
480 by Sanger sequencing of several clones. With the primer pair positioned in exons 20 and 21, we
481 detected amplicons with an exon configuration that matches the expected joining of exons 20
482 and 21 without the intervening exon 20.5 in both the control and PTHS samples (Supplementary
483 Fig. S3a-c), and the percentage of clones supporting the existence of this exon configuration is
484 larger in PTHS than in control samples (Supplementary Fig. S3c), which concurs with the
485 results from rMATS-turbo showing that transcripts with SE-NRXN3-e events are more prevalent
486 than SE-NRXN3-i in PTHS samples. Importantly, the combination of oligos pairing with exons
487 20 and 20.5, which is expected to amplify only the SE-NRXN3-i event-related amplicons,
488 resulted in sequences that match this expected exon configuration in the control samples
489 (Supplementary Fig. S4a-c); moreover, we could only find clones matching this exon
490 configuration in control samples (Supplementary Fig. S3c), which concurs with the positive ΔPSI
491 for the SE-NRXN3-i event in the controls (Fig. 6e). It is also curious to note that, although this
492 type of experiment is not quantitative, the intensity of the 334-bp band with oligos in exons 20
493 and 21 as well as the 252-bp band with oligos in exons 20 and 20.5 are stronger in the control
494 samples (Fig. 7g), which is in keeping with the lower global expression levels for the *NRXN3*
495 gene in PTHS samples revealed by the qPCR experiments (Fig. 7b,c).

496 Although other bands were detected in these PCR experiments, some larger than the predicted
497 size for the corresponding amplicons, they did not yield sequence reads in the Sanger
498 sequencing experiments performed later. The significance of these bands remains to be
499 investigated. In combination, the PCR results presented above confirm the existence of a
500 transcript containing an SE exon in the *NRXN3* gene (SE-NRXN3-i event) identified in silico in
501 our RNA-Seq data and that this splicing event has a lower usage in PTHS neurons, as
502 compared to the transcript without exon 20.5 (SE-NRXN3-e event).

503

504 **The PTHS-depleted alternatively spliced *NRXN3* transcript leads to a prematurely**
505 **stopped soluble Neurexin-3 protein isoform**

506 Next, we investigated the Neurexin-3 protein isoforms coded for by transcripts containing the
507 SE-NRXN3-i and SE-NRXN3-e events. The alternative *NRXN3* Ensembl transcript
508 ENST00000554738.5, containing the splicing configuration with exon 20.5 (SE-NRXN3-i event),

509 which is depleted in PTHS, results in a protein isoform with 6 laminin G domains and 3 EGF-like
510 domains (Fig. 8a), as judged by protein domain prediction with the InterPro tool[49].
511 Comparatively, the canonical *NRXN3* Ensembl transcript ENST00000335750.7 encodes a
512 protein with the same number of protein domains, but shorter C-terminus (Fig. 7A). The shorter
513 protein encoded when exon 20.5 is included results from a premature stop codon in this exon
514 (Fig. 8b). Because Neurexin proteins are transmembrane (TM) cellular components involved in
515 synapse organization[47], with the TM domain positioned near the C-terminus, we reasoned that
516 the shorter Neurexin isoform encoded by the transcript including exon 20.5 might be lacking part
517 of or all the TM domain. Therefore, we conducted a prediction of TM domains using the
518 DeepTMHMM tool[50], which showed that the shorter isoform completely lacks the TM domain
519 and may represent a soluble form of Neurexin (Fig. 8c). Because the balance between a
520 transmembrane and a secreted soluble form of Neurexin may have important functional
521 implications, we checked whether the protein isoforms from the canonical and the alternative
522 *NRNX3* transcripts are predicted to be secreted, using the SignalP (v 6.0) tool[51]. Both the
523 complete Neurexin isoform including exon 20.5 and the shorter isoform encoded by the
524 transcript including exon 20.5 are predicted to be secreted, because they contain a signal
525 peptide (Fig. 8d).

526 To further investigate the Neurexin protein isoforms in neuronal cultures from PTHS patients
527 and controls, we performed Western Blotting with samples harvested from neuronal cultures
528 differentiated over the course of 3 weeks in vitro. Analysis of samples from two PTHS subjects
529 (patients #1 and #2) and a control cell line (control #1) indicates that several protein variants are
530 detected across all samples (Fig. 8e), including a band of molecular weight ~50 kDa (filled
531 arrowhead in Fig. 8e), which likely corresponds to Neurexin-3β[47], the smaller isoform translated
532 from a shorter mRNA transcribed from an internal alternative promoter in the *NRXN3* gene
533 (Supplementary Table S9). This isoform is predicted to have a transmembrane domain and
534 therefore be derived from translation of the transcript not containing exon 20.5 (SE-NRXN3-e
535 splicing event). We could also detect bands of ~40 kDa (open arrowheads in Fig. 8e), which is
536 the predicted molecular weight of Neurexin-3β lacking a transmembrane domain
537 (Supplementary Table S9), resulting from the inclusion of exon 20.5 (SE-NRXN3-i splicing
538 event). We did not detect a band of ~170 kDa, which would correspond to the longest Neurexin-
539 3 isoform, called Neurexin-3α[47], neither could we verify the presence of a band of ~150 kDa,
540 corresponding to the shorter version of Neurexin-3α lacking a transmembrane domain; these
541 isoforms are predicted to be encoded by transcripts lacking or containing exon 20.5,

542 respectively. We verified that the larger ~50 kDa isoform is weaker in PTHS patient #2 sample
543 as compared to the control sample (control #1) (Fig. 8e), in keeping with the observation that
544 the overall *NRXN3* expression levels are reduced in PTHS neurons from patient #2 in qPCR
545 and RNA-Seq experiments (Fig. 7b,c).

546 Importantly, we performed Western Blotting analysis of PTHS and control cortical organoids
547 (see Methods for details) and verified that both the larger ~50 kDa isoform and one of the ~40
548 kDa bands are weaker in PTHS patients #1 and #2 samples as compared to the control sample
549 (Fig. 8f), also in keeping with the observation that *NRXN3* expression is reduced in PTHS
550 neurons from patients #1 and #2 in qPCR and RNA-Seq experiments (Fig. 7b,c). Interestingly,
551 in the PTHS samples, the decrease in intensity for the ~40 kDa band (open arrowhead in Fig.
552 8f) is more pronounced than the drop in intensity for the ~50 kDa band (filled arrowhead), which
553 concurs with our observations that the ratio between the expression levels for the SE-NRXN3-i
554 and SE-NRXN3-e splicing events decreases in patients #1 and #2 PTHS samples in
555 comparison with control #1 (qPCR and rMATS-turbo results in Fig. 7e).

556 In combination, our results point to the higher prevalence of a distinct Neurexin protein isoform
557 due to abnormal splicing patterns, potentially dictated by the dysregulated expression of RBFOX
558 and NOVA1 splicing regulators, in neurons and organoids derived from Pitt-Hopkins Syndrome
559 patients.

560 **DISCUSSION**

561 RNA splicing plays a major role in producing the incredible variety of transcripts and their
562 encoded protein products found in human cells. Yet, how the dysregulation of splicing events
563 lead to disease is a topic that has only recently emerged. Over the last two decades, several
564 studies have sought to elucidate how splicing can go from an important regulatory phenomenon
565 able to regulate human gene expression and generate diverse mature mRNAs to pathogenic
566 altered processes that can contribute to disease onset and progression. Of particular interest
567 are splicing events that lead to exon skipping (ES), intron retention (IR), alternative 5' or 3'
568 splice site usage (A5SS or A3SS), or the use of mutually exclusive exon[7]. Many of these
569 alternative splicing events lead to frameshifts and premature stop codons that result in protein
570 truncation (protein truncating variants; PTV), whose role in neurodevelopmental disorders are
571 becoming increasingly clear[2].

572 Even though the several recognized types of autism are the result of a complex interplay
573 between genetic factors and environmental influences, their pathophysiology is still mostly
574 unknown, and the disease mechanisms remain to be determined in most cases. It is becoming
575 apparent that, among the many molecular features of this complex set of disorders,
576 dysregulation of splicing is a more common phenomenon than initially anticipated[2]. One theme
577 that is starting to be a topic of intense research in the field of autism molecular neurobiology is
578 the decipherment of how altered splicing events or aberrant splicing patterns contribute to the
579 cellular characteristics of the neural tissue in autistic children.

580 In this study, we determined that several genes exhibit aberrant splicing patterns in neurons
581 derived from patients with a monogenic form of autism known as Pitt-Hopkins Syndrome (Figs.
582 3 and 4). We also showed that these altered splicing events are concomitant with the
583 dysregulated expression of NOVA1 and RBFOX1/2/3 splicing regulators (Figs. 1 and 2). These
584 are well known RNA binding proteins (RBPs) that facilitate spliceosome assembly and ensure
585 accurate recognition of splice sites to lead to appropriate intron excision[52,53]. Extensive RBP-
586 RNA interaction experiments have unveiled the participation of NOVA and RBFOX family
587 members in splicing regulation, determining that they are prominently expressed in neurons and
588 crucial to neurogenesis, axon guidance, and synapse formation[2]. An example of a neuronal
589 gene regulated by alternative splicing is *DLG4* (encoding PSD-95), which may generate
590 transcripts via the inclusion of specific exons that result in the incorporation of a domain lacking
591 palmitoylation sites, thereby reducing membrane localization and enhancing excitatory synaptic
592 transmission[54].

593 Importantly, altered splicing in neurons of autistic patients impacts genes involved in
594 neurodevelopment and synaptic plasticity, including synapse-related genes known to be risk
595 factors for autism, such as *NLGN3*, *NLGN4*, *NRXN1*, *SHANK3*, and *CADPS*[55]. Our data showed
596 that one of the aberrant splicing patterns observed in PTHS affect the *NRXN2* and *NRXN3*
597 genes (Fig. 6), which encode Neurexin protein family members. It is interesting to note that
598 altered splicing has been shown to affect the *NRXN1* gene in other forms of autism: these
599 studies have pinpointed the existence of region-specific splicing of *NRXN1* in the prefrontal
600 cortex, potentially influencing synapse formation[56]. Although this splicing event also involves a
601 gene in the Neurexin family, our data show a different case in which a monogenic form of
602 autism, caused by haploinsufficient heterozygous mutations in the *TCF4* gene, lead to changes
603 in RBFOX and NOVA splicing regulators, potentially in turn leading to aberrant splicing patterns
604 involving exon skipping events (Figs. 6 and 7), thereby producing a change in Neurexin 3
605 transcripts that modifies the balance between transmembrane and secreted forms of this
606 synapse-related protein (Figs. 7 and 8).

607 Changes in NOVA and RBFOX expression have been studied by many groups over the last
608 years, showing that these events disrupt neuronal development, leading to neurodevelopmental
609 and neurodegenerative diseases[57]. Other studies further sought to understand how such
610 dysregulation leads to pathological changes in splicing patterns. For example, RBFOX
611 expression was shown to be downregulated in autism, a characteristic that leads to aberrant
612 splicing in several ASD-associated genes in the SFARI database, including *SHANK3*,
613 *CACNA1C*, and *TSC2*[1] and synapse-related genes *NRCAM* and *GRIN1*[58,59]. Moreover,
614 mutations in *NOVA2* have been associated with autism and other neurodevelopmental
615 disorders, impairing neurite outgrowth and axonal pathfinding[60,61]. Thousands of NOVA2 binding
616 sites have been located in the mouse genome, particularly in genes involved in synapse and
617 axon guidance such as *Dcc*, *Robo2*, *Slit2*, and *Epha5*[62,63]. Our study significantly expands these
618 studies by describing that NOVA1 and RBFOX1/2/3 expression are impaired in a monogenic
619 form of autism, PTHS, and by detecting thousands of genes in which splicing patterns are
620 altered (Figs. 3 and 4).

621 It is noteworthy that many genes characterized by aberrant splicing patterns in PTHS are
622 involved in synapse formation and organization (Fig. 4), which prompted us to focus on one
623 particular splicing event (exon skipping) that affects the synapse-related *NRNX3* gene (Fig. 6).
624 This finding may explain the impaired electrical activity we observed in the PTHS neural
625 tissue[34], as judged by the analysis of neurons in traditional 2D culture and in patient-derived

626 brain organoids. These findings concur with our detection of transcript variants derived from
627 alternative splicing in genes in the Neurexin family, which are known to control synapse
628 formation during normal brain development[36,47]. In particular, the *NRXN3* gene encodes two
629 major types of Neurexin, a large isoform encoded by longest isoform including most exons (α
630 Neurexin-3 type) and a short isoform derived from transcription from an internal promoter (β
631 type), both transmembrane-bound proteins[47]. Neurexins interact with Neuroligin proteins to
632 control the rate at which synapses are formed in maturing neurons[64,65].

633 Our study detected a change in the abundances of two transcripts derived from alternative
634 splicing: in neurons of normal genotype, there seems to be an alternative splicing transcript that
635 results from exon exclusion, leading to a α-type Neurexin lacking the transmembrane domain
636 which is expected to be secreted[66]; in contrast, in PTHS neurons, the abundance of this
637 secreted form is diminished relative to the transmembrane form (Fig. 8). Although the transcript
638 with exon exclusion (SE-NRXN3-e) has already been described in the literature[66,67], its
639 involvement in the context of a neurodevelopmental disorder is novel and may open new
640 avenues of investigation to understand how such splicing dysregulation leads to aberrant
641 synapses and altered electrical activity in the neural tissue of autistic children. In the context of a
642 neurodegenerative disorder (Alzheimer's disease), the ratio between the Neurexin-3
643 transmembrane and soluble isoforms was found to be reduced[67], which is exactly in opposition
644 to what we observed in the context of autism. Further studies will illuminate the functional
645 contribution of these ratio alterations in both diseases.

646 Another interesting possibility is that the changes in ratio between the transmembrane and
647 secreted isoforms of Neurexin-3 may lead to differences in the content of GABAergic and
648 glutamatergic synapses in PTHS. We raised this possibility based on the observation that
649 deletion of the *Nrxn3* gene in mice led to a decrease in GABA-mediated inhibitory responses[65].
650 Outstandingly, we observed an augmentation of GABAergic neurons in PTHS cortical
651 organoids, while these cells are mostly lacking in control cortical organoids (Fig. 2b,c,e,g,i), a
652 piece of observation that may explain why PTHS cortical organoids have lower electrical
653 activity[34].

654 In conclusion, our study described alterations in the expression of splicing regulators in PTHS
655 and how this is accompanied by aberrant splicing patterns affecting hundreds of genes involved
656 in neurodevelopment. Further studies are needed to unravel how these alterations contribute to
657 the pathology in autistic brains and to result in the identification of molecular therapeutic targets,

658 eventually leading to the development of strategies to correct abnormalities in splicing regulation
659 in autism.

660 # METHODS

661 ## Patient-derived neural progenitor cell lines and neuronal differentiation

662 Our studies are based on RNA-Seq and single-cell RNA-Seq from our previous publication
663 using neurons and brain organoids derived from patients with PTHS[34]. This study included
664 subjects from volunteering families recruited through the University of Campinas
665 (Supplementary Table 6) harboring heterozygous mutations in *TCF4* mutation. Details on the
666 patients' PTHS clinical symptoms are reported in Supplementary Table 6. Control subjects were
667 the patients' same-sex parents, with no prior history of psychiatric or genetic disorders. The
668 participation of all subjects was approved by the Human Subjects Ethics Committees of the
669 University of Campinas, under CAAE number 86136925.6.0000.5404. Written informed consent
670 was obtained from all participating families after receiving a thorough description of the study
671 and no compensation was provided to participants.

672 In our previous study, neural progenitor cells were obtained from reprogrammed iPSCs derived
673 from skin fibroblasts subjected to cellular reprogramming via over-expression of the Yamanaka
674 factors *OCT4*, *SOX2*, *KLF4*, and *MYC* (Cytotune iPS 2.0 Sendai reprogramming kit; Thermo
675 Fisher Scientific)[34]. All iPSC lines were validated via immunostaining and SNP mapping to rule
676 out the presence of unwanted chromosomal abnormalities and mutations. Results reported in
677 this paper are from experiments conducted with one P15 iPSC clone per subject. Cultures were
678 tested every two weeks for mycoplasma.

679 iPSC colonies maintained in mTeSR1 Plus medium (Stem Cell Technologies), followed by
680 addition of 10 mM SB431542 and 1 mM dorsomorphin to form embryoid bodies. After 2 weeks
681 of culturing, the embryoid bodies were plated onto Matrigel-coated plates with DMEM/F12
682 medium plus N2 and SM1 supplements (Stem Cell Technologies) and 20 ng/mL FGF-2. Neural
683 rosettes were then picked and replated onto Matrigel-coated dishes, and the resulting NPCs
684 were dissociated with Accutase and re-seeded onto plates coated with 10 µg/mL poly-ornithine
685 (Sigma-Aldrich) and 5 µg/mL laminin (Thermo Fisher Scientific).

686 For neuronal differentiation, NPCs were seeded onto plates coated with poly-ornithine and
687 laminin. At 90% confluency, medium was replaced with DMEM/F12 containing N2 and B27
688 supplements (Thermo Fisher Scientific) and 1% penicillin/streptomycin, with media changes
689 occurring every 3 to 4 days.

690

691 **RNA sequencing from NPCs and neuronal cultures and single-cell RNA sequencing data**
692 **from organoids**

693 Our study employed bulk RNA sequencing data from NPCs and neurons derived from PTHS
694 syndrome, which have been previously published by our group[34]. Briefly, these libraries were
695 produced from NPCs of 4 subjects and 4 respective parental controls at passage 15 and from
696 differentiating neuronal cultures of 3 parent-patient pairs and an additional patient line at 2
697 months in vitro. RNA was extracted from 3 independently prepared biological replicates,
698 followed by Illumina library preparation using the stranded TruSeq kit (Illumina) and sequencing
699 on an Illumina NovaSeq 6000 S4 instrument with 150 bp paired-end reads. Transcript-level
700 expression abundance was estimated using Salmon (version 0.14.1) software[68], with selective
701 mapping ('--validateMappings') and correction for sequence-specific biases ('--seqBias'), GC-
702 content biases ('--seqBias'), and fragment position bias ('--posBias'). Reference transcripts for
703 read mapping were obtained from the GENCODE 32 basic annotation[69]. MA plots of specific
704 genes in RNA-Seq data was produced from dataframes containing the expression abundances
705 in each individual library, using the 'ggplot' package for *R* language.

706 Single-cell RNA-Seq data used in this study was also previously published by our team (REF
707 our paper), with samples from cortical organoids (CtOs) and subpallial organoids (sPOs).
708 Briefly, CtOs were produced from iPSC colonies dissociated using Accutase (Thermo Fisher
709 Scientific), followed by neural induction in mTeSR1 Plus medium (Stem Cell Technologies)
710 supplemented with 10 mM SB431542 (Stemgent) and 1 mM dorsomorphin (R&D Systems).
711 Embryoid bodies formed were transferred to Neurobasal medium (Thermo Fisher Scientific)
712 containing GlutaMAX, 1% B27 supplement (Thermo Fisher Scientific), 1% N2 NeuroPlex
713 supplement (Gemini Bio-Products), 1% NEAA (Thermo Fisher Scientific), 1%
714 penicillin/streptomycin (Thermo Fisher Scientific), 10 mM SB431542, and 1 mM dorsomorphin,
715 for 7 days. NPC proliferation medium was then used, consisting of Neurobasal medium
716 containing GlutaMAX, 1% B27, 1% NEAA, 20 ng/mL FGF-2 (Thermo Fisher Scientific) for 7
717 days, followed by 7 additional days with 20 ng/mL EGF (PeproTech). Neuronal differentiation
718 was achieved in Neurobasal medium containing 1% GlutaMAX, 1% Gem21, 1% NEAA, 10
719 ng/mL of BDNF, 10 ng/mL of GDNF, 10 ng/mL of NT-3 (all from PeproTech), 200 mM L-
720 ascorbic acid, and 1 mM dibutyryl-cAMP (Sigma-Aldrich), for 7 days. GABAergic-enriched
721 subpallial organoids (sPOs) were producing using a similar protocol, with neural induction
722 medium containing 5 μM IWP-2 (SelleckChem), from day 4 until day 10, followed by incubation
723 in proliferation medium (Neurobasal medium containing 1% GlutaMAX, 1% Gem21, 1% NEAA,

724 20 ng/mL FGF-2, and 100 nM SAG (SelleckChem) for 7 days, followed by 2 additional days in
725 the same medium supplemented with 20 ng/mL EGF (PeproTech).

726 Single cell RNA-Seq was performed on dissociated CtOs and GbOs at 8 weeks in vitro, with 15
727 organoids per library (5 organoids from each of three wells from independent experiments)
728 dissociated with forceps and enzymatic digestion with Accutase. Libraries were prepared using
729 the Chromium Single Cell 3' v3 Library kit (10× Genomics) according to the manufacturer's
730 protocol, with a target of 20,000 cells per sample on the Chromium chip and PCR-amplification
731 for a total of 10 cycles. Sequencing was performed on a NovaSeq 6000 S4 sequencer (Illumina)
732 to produce 20,000 reads per single cell. Feature count matrices for each single-cell RNA-Seq
733 library were generated separately using the 'cellranger count' command in the Cell Ranger
734 software (version 4.0.0) and the GRCh38 2020-A reference dataset of human transcripts,
735 yielding an estimated number of cells across all libraries in the range 2,944 to 6,466 per library,
736 with a mean number of reads per cell ranging from 58,501 to 169,931. Cell type subpopulations
737 were demarcated via automated annotation and refinement after manual inspection. Seurat
738 (version 3.2.2)[70] was used for producing UMAP and violin plots in this study, after normalization
739 to 10,000 counts per cell and log-transformation with the 'NormalizeData' function, finding of
740 variable features with the 'FindVariableFunctions' function, scaling with the 'ScaleData' function,
741 and linear dimensional reduction (PCA) with the 'RunPCA' function. Non-linear reduction was
742 done using the UMAP algorithm in the 'RunUMAP' function. For statistical comparisons of gene
743 expression levels, we used Mann-Whitney U test.

744

745 **rMATS-turbo analysis of splicing events**

746 rMATS-turbo analysis was conducted using control and patient RNA-seq data previously
747 published by our group (GEO accession numbers GSE159392 and GSE189121)[34]. For
748 alternative splicing analysis conducted with libraries with different read sequence lengths,
749 sequences were trimmed down to the shortest length across all libraries (101 bp) using
750 Trimmomatic software[71]. rMATS-turbo was run using the following arguments: end-pairing ('-t')
751 equal to 'paired', read length ('—readLength') equal to 101 or 151, depending on the library, as
752 well as a function to find novel splice-sites ('—novelSS'). The raw output data was then filtered
753 using rMATS-turbo specific in-built filtering script 'rmats_filtering.py'[72], with parameters set to
754 filter events with a minimum average number of 10 read counts per sample, to filter out events
755 with PSI < 0.05 or > 0.95, to filter events with FDR < 0.05, and to filter events with absolute
756 values of IncLevelDifference (ΔPSI) > 0.05. Over-representation (ORA) and Gene-Set

757 Enrichment Analysis (GSEA) were performed using the lists of genes for which SE events had
758 absolute values of ΔPSI > 0.3, for each patient-control pair, using the WebGestalt software[73]
759 and Gene Ontology - Biological Process and KEGG pathway functional databases, with the
760 'genome protein-coding' reference set. For GSEA, the list of genes was ordered according to
761 the absolute values of IncLevelDifference, with GO-Biological Process and KEGG pathway
762 functional databases.

763

764 **RBP binding site recognition and enrichment analyses**

765 For the analysis of motif enrichment for RBFOX and NOVA regulators, we recovered the
766 genomic coordinates for the list of SE events that had absolute values of ΔPSI > 0.1, for patient-
767 control pair #2. To recover the sequences of the exons involved in these SE events plus 200 bp
768 of the neighboring introns, we subtracted 199 from the value of the initial exonic genomic
769 coordinate ('exonStart_0base' column in the rMATS-turbo output table) and added 200 to the
770 value of the final exonic genomic coordinate ('exonEnd' column). Sequences were recovered in
771 fasta format using the 'faidx' function in samtools[74] from the GRCh38 human genome database.
772 RBP motif enrichment was conducted using the SEA software in the MEME suite[43], with RNA
773 motif database 'Ray2013_rbp_Homo_sapiens.dna_encoded.meme', which was modified to
774 include motifs for NOVA1, RBFOX2, and RBFOX3. A position-specific scoring matrix (PSSM)
775 for NOVA1 was obtained from the RBPmap developing team[75,76]; PSSM for RBFOX2 and
776 RBFOX3 were produced using the 'matrix2meme' script in the MEME suite using published
777 motif sequences from RNA Bind-n-Seq (RBNS) results (Supplementary Table S3 in ref[44]). SEA
778 was run using default parameters plus arguments to avoid trimming ('--notrim') and the '--
779 hofract' parameter set to 0.5. As a negative control sequence set, we started with a random
780 selection of 5,000 exons collected across all genes in the GRCh38 database using 'awk', 'sort',
781 and 'head', to produce a FASTA file with exonic and neighboring intronic (200 bp) sequences.
782 As positive control sequences for RBFOX1/2/3 and NOVA1, we selected genes whose splicing
783 is known to regulated by these proteins[2,77] and recovered all exonic plus neighboring intronic
784 (200 bp) sequences.

785 For the detection of binding sites of NOVA1 and RBFOX1/2/3 in specific genes (including
786 *NRXN3*), we first obtained the FASTA files for the target genes from Ensembl (genome
787 assembly GRCh38.p14; GCA_000001405.29) and then run the motif search using Find
788 Individual Motif Occurrences (FIMO) software in the MEME suite[45], with the '--norc' argument to
789 prevent motif scanning in the reverse complement strand. We ran this analysis for 50 genes at

790 the top of the SE event list from rMATS-turbo, ordered according to the absolute values of ΔPSI.
791 In parallel, we ran FIMO scanning for 50 random genes that were not found in the rMATS-turbo
792 output SE event list. The frequencies of RBP binding sites were then normalized to 100,000 bp,
793 followed by enrichment analysis using unpaired *t*-test in GraphPad Prism.

794

795 **PCR and sequencing of cloned bands**

796 PCR was conducted using GoTaq DNA polymerase (Promega; cat# M3001) with primers p6 (5'
797 TCTGCTGAATGTTCAAGTG 3') and p7 (5' TCTTCAGTTTGGTGCTGTC 3') for the first
798 reaction and primers p6 and p8 (5' GGAGATGGATGACAGCAC 3') for the second reaction (Fig.
799 7f,g), using the following cycling parameters: 94°C 5 min, and 38 cycles of 94°C 45 s, 58°C 45 s,
800 and 72°C 2 min. The fragments were then cloned into the pGEM-T-easy vector (Promega) and
801 Sanger sequenced using universal M13 primer. Alignment was performed using Benchling
802 alignment tool.

803

804 **Protein secondary structure analysis**

805 Protein secondary structure analysis was performed using InterProScan[49] for general domain
806 prediction using the coding amino acid sequence of *NRXN3* ENST00000335750.7 and
807 ENST00000554738.5 transcripts, representing the transmembrane and soluble isoforms,
808 respectively, using default parameters. Specific transmembrane domain prediction was
809 performed using DeepTMHMM 1.0 software[50], inputting the same sequences mentioned above.
810 The likelihood of secretion was evaluated using the SecretomeP (v 2.0) tool

811

812 **Real-time quantitative qPCR**

813 For real-time qPCR, neuronal cultures were differentiated from NPCs seeded onto 6-well plates,
814 followed by withdrawal of FGF-2 for 3 weeks, prior to RNA extraction with the RNeasy Mini Plus
815 kit (Qiagen). All samples were analyzed with 3 independent biological replicates. cDNA was
816 synthesized from total RNA using the Improm II First-Strand Reverse Transcription System
817 (Promega). Real-time quantitative PCR (RT-qPCR) was performed using regular primers for
818 SYBR Green technology, on an Applied Biosystems Real Time PCR system, with the following
819 cycling parameters: 94°C for 3 min, followed by 40 cycles of 94°C for 30 s and 68°C for 1 min.
820 Amplification and denaturation curves for all probes were analyzed to verify amplification of just

821 one amplicon. Normalization was achieved with endogenous control gene *ACTB*, and relative
822 expression was calculated using the traditional ΔΔCt method. The following qPCR primers were
823 used to detect all *NRXN3* transcript variants: p1 (5' ACAACCCGTAAGAATGCGTC 3') and p2
824 (5' CATCACTTGAACATTCAGCAG 3'). The following variant-specific qPCR primers were used:
825 p1, p3 (5' GGAAAGACTCTTATCTGTACTC 3'), p4 (5' TAGAGCTTCTGGCTGTACTC 3'), and
826 p5 (5' CGTAAGAATGCGCTCTACAG 3').

827

828 **Cortical organoid derivation**

829 For the generation of cortical brain organoids, we used our previously published protocol. iPSC
830 colonies were dissociated using Accutase (Thermo Fisher Scientific; diluted with an equal
831 volume of 1× PBS) for 12 min at 37 °C, followed by centrifugation for 3 min at 150 × *g*. Next,
832 dissociated cells were resuspended in mTeSR Plus medium (Stem Cell Technologies) with
833 10 mM SB431542 (Stemgent) and 1 mM dorsomorphin (R&D Systems), followed by seeding 3–
834 4 million cells onto low-binding 6-well plates. Organoids were cultured for 1 month on a shaker
835 inside a CO_2 incubator at 95 rpm. Rho kinase inhibitor (Y-27632; Calbiochem, Sigma-Aldrich)
836 was added at a 5 mM concentration during the first 24 hours, in mTeSR Plus medium, which
837 was supplemented with 10 mM SB431542 and 1 mM dorsomorphin; the same medium without
838 Rho kinase inhibitor continued to be used for an additional 2 days. Next, medium was replaced
839 with Neurobasal medium (Thermo Fisher Scientific) containing GlutaMAX, B27 supplement
840 (Thermo Fisher Scientific), 1% N2 supplement (Thermo Fisher Scientific), 1% NEAA (Thermo
841 Fisher Scientific), 1% penicillin/streptomycin (Thermo Fisher Scientific), 10 mM SB431542, and
842 1 mM dorsomorphin, for 5 days, with the addition of Rho kinase inhibitor on the first day of
843 neural induction phase. Medium was then replaced with Neurobasal medium containing
844 GlutaMAX, B27, 1% NEAA, penicillin/streptomycin, and 20 ng/mL FGF-2 (Thermo Fisher
845 Scientific) for 8 days, followed by 6 additional days in the same medium further supplemented
846 with 20 ng/mL EGF (PeproTech). Next, we used a transition phase by incubating the organoids
847 in Neurobasal medium containing 1% GlutaMAX, 1% B27, 1% NEAA, penicillin/streptomycin for
848 3 days, followed by the neuronal differentiation and organoid maturation phase in Neurobasal
849 medium containing 1% GlutaMAX, 1% B27, 1% NEAA, penicillin/streptomycin, 10 ng/mL of
850 BDNF, 10 ng/mL of GDNF, and 10 ng/mL of NT-3 (all from PeproTech), for the remainder of the
851 derivation protocol.

852

853 **Western Blotting**

854 For Western Blotting analysis of Neurexin-3 isoforms, neuronal cultures were differentiated from
855 NPCs seeded onto 6-well plates, followed by withdrawal of FGF-2 for 3 weeks, prior to protein
856 extraction in RIPA buffer (0.05 M Tris-Cl pH 7.4; 1 M NaCl; 1% SDS) containing Protease
857 Inhibitor Cocktail (Thermo Fisher Scientific), with mechanical dislodging of cells with a cell
858 scraper. We also used organoid samples at 1 month in vitro, which were crushed in RIPA buffer
859 containing protease inhibitor cocktail with the help of a plastic pistil. The crude extracts were
860 clarified by centrifugation at 10,000 × *g* for 5 min, followed by discontinuous SDS-PAGE
861 separation of proteins using a 7% acrylamide resolving gel, with 30 μg of total protein per
862 sample. After protein transfer onto nitrocellulose membranes (Hybond-C; Amersham) using a
863 TransBlot SD semi-dry transfer cell (BioRad), the membrane was blocked using TBS buffer (20
864 mM Tris-Cl pH 7.4; 150 mM NaCl) containing 0.1% Tween-20 (Sigma) and 3% BSA (Sigma),
865 followed by detection of Neurexin-3 target proteins by incubation with primary antibody for 16 h
866 at 4°C (anti-Neurexin-3 (E7K3G) rabbit monoclonal antibody; #48004S; Cell Signaling
867 Technology; 1:1000) and fluorescent secondary antibody (IRDye 800CW goat anti-rabbit IgG.
868 LiCOR; 1:5,000). Development was performed on an iBright CL1500 Imaging System (Thermo
869 Fisher Scientific). As endogenous control, we used a mouse anti-GAPDH primary antibody
870 (#60004; Proteintech; 1:2000) and secondary detection with IRDye 680CW goat anti-mouse
871 antibody (LiCOR; 1:5,000).

872

873 **Statistical analysis and reproducibility**

874 Data are presented as mean + SEM, unless otherwise indicated. Different types of statistical
875 test were used throughout the study, including comparisons of means between two groups
876 (PTHS against parent) in experiments that measured relative expression levels, or expression
877 abundances used two-sample Welch's t test, assuming unequal variances and
878 heteroskedasticity. For comparing mean gene expression in single cell RNA-Seq data between
879 two samples, we used the non-parametric Mann–Whitney U-test. Sample sizes are indicated in
880 the figure legends. *P*-values are reported as asterisks in the figures for significance levels
881 defined as $p<0.05$ (*), $p<0.01$ (**), or $p<0.001$ (***). Supplementary Table S8 presents extended
882 results for all statistical tests performed, including sample sizes, statistical tests employed, effect
883 sizes, statistics metrics (*H, F, t*, or *W*), along with exact *p*-values, listed according to the order of
884 appearance in figure panels throughout the study. The numbers of replicates are also indicated
885 in the figure legends and all attempts at replication were successful. When experiments involved

886 data collected from independent biological replicates, results were collected from randomly
887 chosen replicates (wells/plates of experiments involving cells in 2D culture) and blinding was
888 used for most analyses comparing patients and control samples, including immunostaining.
889 Blinding was not used when analyzing results from RNA sequencing and single cell RNA
890 sequencing experiments, due to the inherently unbiased nature of the bioinformatic approaches
891 used for quantitating gene expression and determining differential expression between
892 genotypes or cell types. Statistical analyses were performed using Prism software (GraphPad;
893 version 9.2.0). Figures were composed with Prism and Illustrator CS4 (Adobe; version 14.0.0).

894 **Materials Availability**

895 Further information and requests for resources and reagents should be directed to and will be
896 fulfilled by the corresponding author, Fabio Papes (papesf@unicamp.br), upon reasonable
897 request. When provided to others, unique reagents generated in this study will be available with
898 a completed Materials Transfer Agreement.

899

900 **Data Availability**

901 Data supporting the findings in this study are included within the Supplementary Material. RNA
902 sequencing and single cell RNA sequencing raw and processed data used in this study are
903 deposited at the Gene Expression Omnibus (GEO) of the National Center for Biotechnology
904 Information (NCBI), under accession numbers GSE159392
905 (https://www.ncbi.nlm.nih.gov/geo/query/acc.cgi?acc=GSE159392), GSE159859
906 (https://www.ncbi.nlm.nih.gov/geo/query/acc.cgi?acc=GSE159859), GSE159860
907 (https://www.ncbi.nlm.nih.gov/geo/query/acc.cgi?acc=GSE159860), and GSE189121
908 (https://www.ncbi.nlm.nih.gov/geo/query/acc.cgi?acc=GSE189121), which are available publicly
909 without restriction.

910

911 **Code Availability**

912 No new custom software or code has been used in this paper. Codes (R programming
913 language) used for bioinformatic analyses are all strictly based on pre-existing, regularly used
914 published codes for RNA-Seq and single-cell RNA-Seq analyses, as described above.

915 ## References

916 1. Weyn-Vanhentenryck, S. M. *et al.* HITS-CLIP and Integrative Modeling Define the Rbfox Splicing-
917 Regulatory Network Linked to Brain Development and Autism. *Cell Rep* **6**, 1139–1152 (2014).

918 2. Jeong, J., Yoo, H. J., An, J. Y. & Jeong, S. Dysregulated RNA-binding proteins and alternative
919 splicing: Emerging roles in autism spectrum disorder. *Mol Cells* **48**, 100237 (2025).

920 3. Kjer-Hansen, P. & Weatheritt, R. J. The function of alternative splicing in the proteome: rewiring
921 protein interactomes to put old functions into new contexts. *Nature Structural & Molecular*
922 *Biology 2023 30:12* **30**, 1844–1856 (2023).

923 4. Zheng, S. Alternative splicing programming of axon formation. *Wiley Interdiscip Rev RNA* **11**,
924 e1585 (2020).

925 5. Quesnel-Vallières, M., Weatheritt, R. J., Cordes, S. P. & Blencowe, B. J. Autism spectrum disorder:
926 insights into convergent mechanisms from transcriptomics. *Nature Reviews Genetics 2018 20:1*
927 **20**, 51–63 (2018).

928 6. Kim, K. K., Adelstein, R. S. & Kawamoto, S. Identification of neuronal nuclei (NeuN) as Fox-3, a
929 new member of the Fox-1 gene family of splicing factors. *Journal of Biological Chemistry* **284**,
930 31052–31061 (2009).

931 7. Jacko, M. *et al.* Rbfox Splicing Factors Promote Neuronal Maturation and Axon Initial Segment
932 Assembly. *Neuron* **97**, 853-868.e6 (2018).

933 8. An, J. Y. *et al.* Towards a molecular characterization of autism spectrum disorders: An exome
934 sequencing and systems approach. *Transl Psychiatry* **4**, (2014).

935 9. Teplova, M. *et al.* Protein-RNA and protein-protein recognition by dual KH1/2 domains of the
936 neuronal splicing factor Nova-1. *Structure* **19**, 930–944 (2011).

937 10. Scala, M. *et al.* De novo truncating NOVA2 variants affect alternative splicing and lead to
938 heterogeneous neurodevelopmental phenotypes. *Hum Mutat* **43**, 1299–1313 (2022).

939 11. Licatalosi, D. D. *et al.* HITS-CLIP yields genome-wide insights into brain alternative RNA
940 processing. *Nature* **456**, 464–469 (2008).

941 12. O'Leary, A. *et al.* Behavioural and functional evidence revealing the role of RBFOX1 variation in
942 multiple psychiatric disorders and traits. *Mol Psychiatry* **27**, 4464 (2022).

943 13. Brockschmidt, A. *et al.* Severe mental retardation with breathing abnormalities (Pitt-Hopkins
944 syndrome) is caused by haploinsufficiency of the neuronal bHLH transcription factor TCF4. *Hum*
945 *Mol Genet* **16**, 1488–94 (2007).

946 14. Amiel, J. *et al.* Mutations in TCF4, Encoding a Class I Basic Helix-Loop-Helix Transcription Factor,
947 Are Responsible for Pitt-Hopkins Syndrome, a Severe Epileptic Encephalopathy Associated with
948 Autonomic Dysfunction. *The American Journal of Human Genetics* **80**, 988–993 (2007).

949 15. Zweier, C. *et al.* Haploinsufficiency of TCF4 Causes Syndromal Mental Retardation with
950 Intermittent Hyperventilation (Pitt-Hopkins Syndrome). *The American Journal of Human Genetics*
951 **80**, 994–1001 (2007).

952 16. Pitt, D. & Hopkins, I. A syndrome of mental retardation, wide mouth and intermittent
953 overbreathing. *Aust Paediatr J* **14**, 182–184 (1978).

954 17. Kim, H., Berens, N. C., Ochandarena, N. E. & Philpot, B. D. Region and Cell Type Distribution of
955 TCF4 in the Postnatal Mouse Brain. *Front Neuroanat* **14**, (2020).

956 18. de Pontual, L. *et al.* Mutational, functional, and expression studies of the TCF4 gene in Pitt-
957 Hopkins syndrome. *Hum Mutat* **30**, 669–76 (2009).

958 19. Jung, M. *et al.* Analysis of the expression pattern of the schizophrenia-risk and intellectual
959 disability gene TCF4 in the developing and adult brain suggests a role in development and
960 plasticity of cortical and hippocampal neurons. *Mol Autism* **9**, 1–15 (2018).

961 20. Sepp, M., Kannike, K., Eesmaa, A., Urb, M. & Timmusk, T. Functional Diversity of Human Basic
962 Helix-Loop-Helix Transcription Factor TCF4 Isoforms Generated by Alternative 5' Exon Usage and
963 Splicing. *PLoS One* **6**, e22138 (2011).

964 21. Chen, E. S. *et al.* Molecular convergence of neurodevelopmental disorders. *Am J Hum Genet* **95**,
965 490–508 (2014).

966 22. Schmidt-Edelkraut, U., Daniel, G., Hoffmann, A. & Spengler, D. Zac1 Regulates Cell Cycle Arrest in
967 Neuronal Progenitors via Tcf4. *Mol Cell Biol* **34**, 1020–1030 (2014).

968 23. Hill, M. J. *et al.* Knockdown of the schizophrenia susceptibility gene TCF4 alters gene expression
969 and proliferation of progenitor cells from the developing human neocortex. *Journal of Psychiatry*
970 *and Neuroscience* **42**, 181–188 (2017).

971 24. Forrest, M. P. *et al.* The Psychiatric Risk Gene Transcription Factor 4 (TCF4) Regulates
972 Neurodevelopmental Pathways Associated With Schizophrenia, Autism, and Intellectual
973 Disability. *Schizophr Bull* **44**, 1100–1110 (2018).

974 25. Page, S. C. *et al.* The schizophrenia-and autism-associated gene, transcription factor 4 regulates
975 the columnar distribution of layer 2/3 prefrontal pyramidal neurons in an activity-dependent
976 manner. *Mol Psychiatry* **23**, 304–315 (2018).

977 26. Fischer, B. *et al.* E-proteins orchestrate the progression of neural stem cell differentiation in the
978 postnatal forebrain. *Neural Dev* **9**, 23 (2014).

979 27. Marangi, G. & Zollino, M. Pitt-Hopkins Syndrome and Differential Diagnosis: A Molecular and
980 Clinical Challenge. *J Pediatr Genet* **4**, 168–76 (2015).

981 28. Zollino, M. *et al.* Diagnosis and management in Pitt-Hopkins syndrome: First international
982 consensus statement. *Clin Genet* **95**, 462–478 (2019).

983 29. Stefansson, H. *et al.* Common variants conferring risk of schizophrenia. *Nature* **460**, 744–747
984 (2009).

985 30. Ripke, S. *et al.* Genome-wide association study identifies five new schizophrenia loci. *Nat Genet*
986 **43**, 969–976 (2011).

987 31. Smoller, J. W. *et al.* Identification of risk loci with shared effects on five major psychiatric
988 disorders: a genome-wide analysis. *The Lancet* **381**, 1371–1379 (2013).

989 32. Wray, N. R. *et al.* Genome-wide association analyses identify 44 risk variants and refine the
990 genetic architecture of major depression. *Nat Genet* **50**, 668–681 (2018).

991 33. Gelernter, J. *et al.* Genome-wide association study of post-traumatic stress disorder
992 reexperiencing symptoms in >165,000 US veterans. *Nat Neurosci* **22**, 1394–1401 (2019).

993 34. Papes, F. *et al.* Transcription Factor 4 loss-of-function is associated with deficits in progenitor
994 proliferation and cortical neuron content. *Nat Commun* **13**, (2022).

995 35. Teixeira, J. R., Szeto, R. A., Carvalho, V. M. A., Muotri, A. R. & Papes, F. Transcription factor 4 and
996 its association with psychiatric disorders. *Transl Psychiatry* **11**, (2021).

997 36. Gomez, A. M., Traunmüller, L. & Scheiffele, P. Neurexins: Molecular Codes for Shaping Neuronal
998 Synapses. *Nat Rev Neurosci* **22**, 137 (2021).

999 37. Trujillo, C. A. *et al.* Complex Oscillatory Waves Emerging from Cortical Organoids Model Early
1000 Human Brain Network Development. *Cell Stem Cell* **25**, 558-569.e7 (2019).

1001 38. Yoon, S.-J. *et al.* Reliability of human cortical organoid generation. *Nat Methods* **16**, 75–78 (2019).

1002 39. Gasiorowska, A. *et al.* The Biology and Pathobiology of Glutamatergic, Cholinergic, and
1003 Dopaminergic Signaling in the Aging Brain. *Front Aging Neurosci* **13**, 654931 (2021).

1004 40. Sun, L. *et al.* Transcriptomic insights into fate choice of pallial versus subpallial GABAergic
1005 neurons. *Nature Communications* **16**, 1–20 (2025).

1006 41. Wang, Y. *et al.* rMATS-turbo: an efficient and flexible computational tool for alternative splicing
1007 analysis of large-scale RNA-seq data. *Nature Protocols 2024 19:4* **19**, 1083–1104 (2024).

1008 42. Wang, J., Vasaikar, S., Shi, Z., Greer, M. & Zhang, B. WebGestalt 2017: a more comprehensive,
1009 powerful, flexible and interactive gene set enrichment analysis toolkit. *Nucleic Acids Res* **45**,
1010 W130–W137 (2017).

1011 43. Bailey, T. L. & Grant, C. E. SEA: Simple Enrichment Analysis of motifs. *bioRxiv* 2021.08.23.457422
1012 (2021) doi:10.1101/2021.08.23.457422.

1013 44. Dominguez, D. *et al.* Sequence, Structure, and Context Preferences of Human RNA Binding
1014 Proteins. *Mol Cell* **70**, 854-867.e9 (2018).

1015 45. Grant, C. E., Bailey, T. L. & Noble, W. S. FIMO: scanning for occurrences of a given motif.
1016 *Bioinformatics* **27**, 1017–1018 (2011).

1017 46. Yuan, Y. *et al.* Cell type-specific CLIP reveals that NOVA regulates cytoskeleton interactions in
1018 motoneurons. *Genome Biol* **19**, 1–19 (2018).

1019 47. Zhang, R., Jiang, H. X., Liu, Y. J. & He, G. Q. Structure, function, and pathology of Neurexin-3.
1020 *Genes Dis* **10**, 1908–1919 (2023).

1021 48. Hishimoto, A. *et al.* Neurexin 3 polymorphisms are associated with alcohol dependence and
1022 altered expression of specific isoforms. *Hum Mol Genet* **16**, 2880–2891 (2007).

1023 49. Blum, M. *et al.* InterPro: the protein sequence classification resource in 2025. *Nucleic Acids Res*
1024 **53**, D444–D456 (2025).

1025 50. Hallgren, J. *et al.* DeepTMHMM predicts alpha and beta transmembrane proteins using deep
1026 neural networks. *bioRxiv* 2022.04.08.487609 (2022) doi:10.1101/2022.04.08.487609.

1027 51. Teufel, F. *et al.* SignalP 6.0 predicts all five types of signal peptides using protein language
1028 models. *Nat Biotechnol* **40**, 1023–1025 (2022).

1029 52. Kumari, A., Sedehizadeh, S., Brook, J. D., Kozlowski, P. & Wojciechowska, M. Differential fates of
1030 introns in gene expression due to global alternative splicing. *Hum Genet* **141**, 31–47 (2022).

1031 53. Jeong, S. SR Proteins: Binders, Regulators, and Connectors of RNA. *Mol Cells* **40**, 1–9 (2017).

1032 54. Han, K. & Kim, E. Synaptic adhesion molecules and PSD-95. *Prog Neurobiol* **84**, 263–283 (2008).

1033 55. Quesnel-Vallières, M., Weatheritt, R. J., Cordes, S. P. & Blencowe, B. J. Autism spectrum disorder:
1034 insights into convergent mechanisms from transcriptomics. *Nat Rev Genet* **20**, 51–63 (2019).

1035 56. Fuccillo, M. V. *et al.* Single-Cell mRNA Profiling Reveals Cell-Type-Specific Expression of Neurexin
1036 Isoforms. *Neuron* **87**, 326–340 (2015).

1037 57. Parra, A. S. & Johnston, C. A. Emerging Roles of RNA-Binding Proteins in Neurodevelopment. *J*
1038 *Dev Biol* **10**, (2022).

1039 58. An, J. Y. *et al.* Towards a molecular characterization of autism spectrum disorders: an exome
1040 sequencing and systems approach. *Transl Psychiatry* **4**, (2014).

1041 59. Voineagu, I. *et al.* Transcriptomic analysis of autistic brain reveals convergent molecular
1042 pathology. *Nature* **474**, 380–386 (2011).

1043 60. Mattioli, F. *et al.* De Novo Frameshift Variants in the Neuronal Splicing Factor NOVA2 Result in a
1044 Common C-Terminal Extension and Cause a Severe Form of Neurodevelopmental Disorder. *Am J*
1045 *Hum Genet* **106**, 438–452 (2020).

1046 61. Scala, M. *et al.* De novo truncating NOVA2 variants affect alternative splicing and lead to
1047 heterogeneous neurodevelopmental phenotypes. *Hum Mutat* **43**, 1299–1313 (2022).

1048 62. Licatalosi, D. D. *et al.* HITS-CLIP yields genome-wide insights into brain alternative RNA
1049 processing. *Nature* **456**, 464–469 (2008).

1050 63. Ule, J. *et al.* CLIP identifies Nova-regulated RNA networks in the brain. *Science* **302**, 1212–1215
1051 (2003).

1052 64. Graf, E. R., Zhang, X., Jin, S. X., Linhoff, M. W. & Craig, A. M. Neurexins Induce Differentiation of
1053 GABA and Glutamate Postsynaptic Specializations via Neuroligins. *Cell* **119**, 1013 (2004).

1054 65. Südhof, T. C. Synaptic Neurexin Complexes: A Molecular Code for the Logic of Neural Circuits. *Cell*
1055 **171**, 745 (2017).

1056 66. Hishimoto, A. *et al.* Neurexin 3 polymorphisms are associated with alcohol dependence and
1057 altered expression of specific isoforms. *Hum Mol Genet* **16**, 2880–2891 (2007).

1058 67. Hishimoto, A. *et al.* Neurexin 3 transmembrane and soluble isoform expression and splicing
1059 haplotype are associated with neuron inflammasome and Alzheimer's disease. *Alzheimers Res*
1060 *Ther* **11**, (2019).

1061 68. Patro, R., Duggal, G., Love, M. I., Irizarry, R. A. & Kingsford, C. Salmon provides fast and bias-
1062 aware quantification of transcript expression. *Nat Methods* **14**, 417–419 (2017).

1063 69. Frankish, A. *et al.* GENCODE reference annotation for the human and mouse genomes. *Nucleic*
1064 *Acids Res* **47**, D766–D773 (2019).

1065 70. Sun, A. X. *et al.* Potassium channel dysfunction in human neuronal models of Angelman
1066 syndrome. *Science (1979)* **366**, 1486–1492 (2019).

1067 71. Bolger, A. M., Lohse, M. & Usadel, B. Trimmomatic: a flexible trimmer for Illumina sequence data.
1068 *Bioinformatics* **30**, 2114 (2014).

1069 72. Wang, Y. *et al.* rMATS-turbo: an efficient and flexible computational tool for alternative splicing
1070 analysis of large-scale RNA-seq data. *Nat Protoc* **19**, 1083–1104 (2024).

1071 73. Elizarraras, J. M. *et al.* WebGestalt 2024: faster gene set analysis and new support for
1072 metabolomics and multi-omics. *Nucleic Acids Res* **52**, W415–W421 (2024).

1073 74. Danecek, P. *et al.* Twelve years of SAMtools and BCFtools. *Gigascience* **10**, 1–4 (2021).

1074 75. Paz, I., Argoetti, A., Cohen, N., Even, N. & Mandel-Gutfreund, Y. RBPmap: A Tool for Mapping and
1075 Predicting the Binding Sites of RNA-Binding Proteins Considering the Motif Environment.
1076 *Methods Mol Biol* **2404**, 53–65 (2022).

1077 76. Paz, I., Kosti, I., Ares, M., Cline, M. & Mandel-Gutfreund, Y. RBPmap: A web server for mapping
1078 binding sites of RNA-binding proteins. *Nucleic Acids Res* **42**, (2014).

1079 77. Piton, A. NOVA1/2 genes and alternative splicing in neurodevelopment. *Curr Opin Genet Dev* **93**,
1080 (2025).

1081 78. Abrahams, B. S. *et al.* SFARI Gene 2.0: a community-driven knowledgebase for the autism
1082 spectrum disorders (ASDs). *Mol Autism* **4**, 36 (2013).

1083

1084

Acknowledgments

We thank Drs. Gonçalo Pereira, J. Andrés Yunes, and Maria Andreia Delbin for resources, Ana Paula Ferreira and Welbe Bragança for administrative and technical help, Dr. Elsa Molina (former director of the UCSD Stem Cell Genomics Core) for technical assistance with single cell RNA-Seq (made possible in part by CIRM Major Facilities grant #FA1-00607 to the Sanford Consortium for Regenerative Medicine). This work was supported by Sao Paulo Research Foundation (FAPESP) grants (#2020/11451-7 and #2022/12762-1), by FAPESP fellowships (#2024/18734-5 to P.K.K.F., #2024/12825-9 to B.B.H., #2025/09026-0 to J.G.B., #2024/20077-2 to G.D.V., and #2020/16525-9 to I.C.V.), and by a CNPq fellowship (L.L.D.). We would also like to thank Yael Mandel-Gutfreund and Dina Alexandrovich (RBPmap team[76]) for providing the NOVA1 motif PSSM.

Author contributions

Conceptualization, F.P.; Methodology, F.P., P.K.K.F., A.P.C., and M.C.; Investigation, P.K.K.F., L.L.D., B.B.H., J.G.B., G.D.V., I.C.V., and M.H.B.; Writing – Original Draft, F.P., P.K.K.F.; Writing – Review & Editing, F.P. and P.K.K.F.; Funding Acquisition, F.P.; Resources, F.P., M.H.B., and M.C.; Supervision, F.P.

Competing interests

Authors declare no competing interests.

1105 ## Figure legends

1106 **Figure 1: Lower expression of splicing regulators NOVA1 and RBFOX1/2/3 in neurons**
1107 **derived from Pitt-Hopkins Syndrome (PTHS) patients. (a-c)** MA plots showing differential
1108 gene expression in neurons in 2D culture in the comparison between different pairs of control
1109 and PTHS subjects – pair #1 in (a), pair #2 in (b) and pair #3 in (c). See Supplementary Table
1110 S6 for patient information. Each parent-patient comparison is shown separately. Gray dots are
1111 genes that are not statistically significantly differentially expressed between control and PTHS.
1112 Colored dots are statistically significant DE genes, and the color indicates adjusted *p*-value (*s*-
1113 value). Red dots represent genes coding for splicing regulators NOVA1, RBFOX1, RBFOX2,
1114 and RBFOX3. The *x* axes represent average normalized expression across all libraries. Fold-
1115 changes (in log scale, base 2) in the *y* axes indicate the contrast between expression levels in
1116 the PTHS patient and the corresponding control (negative values indicate lower expression in
1117 PTHS neurons). **(d)** Summary of fold changes (in log scale, base 2) of *NOVA1* and *RBFOX1/2/3*
1118 gene expression for each patient-parent pair. Symbols indicate different pairs, as shown in
1119 Supplementary Table S6. **(e-h)** MA plots showing differential gene expression in neural
1120 progenitor cells in 2D culture in the comparison between different pairs of control and PTHS
1121 subjects – pair #1 in (e), pair #2 in (f), pair #3 in (g), and pair #4 in (h). **(i)** Summary of fold
1122 changes of *NOVA1* and *RBFOX1/2/3* gene expression in neural progenitor cells. Notice the lack
1123 of change in expression of some of these splicing regulators in neural progenitors. **(j,k)** Relative
1124 expression levels for *NOVA1*, *RBFOX1*, *RBFOX2*, and *RBFOX3* genes, as determined from RT-
1125 qPCR experiments, in iPSC-derived neuronal cultures. Three patients per graph, with mean
1126 expression normalized to 1 in control #1 (j) or control #2 (k). N = 2 technical replicates per
1127 sample. Bar graphs represent mean + SEM. ns, not statistically significantly different, *$p<0.05$,
1128 **$p<0.01$, ***$p<0.001$; two-sample Welch's t-test assuming unequal variances.

1129 **Figure 2: Aberrant expression of splicing regulators in PTHS cortical and subpallial**
1130 **organoids. (a)** Uniform Manifold Approximation and Projection (UMAP) bidimensional reduction
1131 of scRNA-Seq profiling of cortical (CtO) and subpallial (sPO) organoids at 8 weeks in vitro, with
1132 pooled cells from 15 organoids per library. Color code represents 6 annotated subpopulations:
1133 Pr-Glut: neural progenitors in glutamatergic lineage; IP-Glut: intermediate progenitors in
1134 glutamatergic lineage; N-Glut: glutamatergic neurons; Pr-GABA: neural progenitors in inhibitory
1135 lineage; IP-GABA: intermediate progenitors in inhibitory lineage; N-GABA: neuronal population
1136 containing GABAergic interneurons. Minority subpopulations exist but were not the focus of our
1137 study. **(b)** UMAP of annotated cells in CtO and sPO organoids, separated according to organoid
1138 type, showing prevalence of excitatory neuron lineage in CtOs and preponderance of
1139 GABAergic interneurons in sPO libraries. **(c-j)** UMAPs showing expression of *NOVA1* (c,d),
1140 *RBFOX1* (e,f), *RBFOX2* (g,h), and *RBFOX3* (i,j), in control and PTHS CtOs and sPOs. Warmer
1141 colors indicate higher expression levels for each gene, while black indicates absence of
1142 detectable expression.

1143 **Figure 3: Altered percentage of cells expressing splicing regulators in PTHS organoids**.
1144 **(a-d)** Left graphs in each group: Violin plots showing comparison of expression of *NOVA1* (a),
1145 *RBFOX1* (b), *RBFOX2* (c), and *RBFOX3* (d) between N-Glut subpopulations in the parent and
1146 PTHS CtOs (left groups) or between N-GABA subpopulations in the parent and PTHS sPOs
1147 (right groups). N = 1401 (parent) or 380 (PTHS) N-Glut cells, or N = 2661 (parent) and 988
1148 (PTHS) N-GABA cells. Right graphs in each group: changes in percentages of neuronal
1149 subtypes in the analyzed subpopulations of CtOs and sPOs (cells expressing each gene above
1150 threshold corresponding to 0.5 log-normalized expression levels).

1151 **Figure 4: Genes exhibiting aberrant splicing patterns in PTHS are involved in synapse**
1152 **formation and cell-cell communication. (a)** Pie charts representing the distribution of splicing
1153 events in 5 alternative splicing categories, in several pairs of patient and control samples. **(b)**
1154 Pie chart indicating the number of events in each alternative splicing category for the common
1155 splicing events across all patient-control pairs. **(c)** Pie chart representing the number of genes
1156 for which splicing events were detected in each alternative splicing category, in the intersection
1157 across all patient-control pairs. **(d,e)** Enrichment ratios observed in Over-Representation
1158 Analysis (ORA) of splicing events with an absolute value of DPSI larger than 0.3 in the patient-
1159 control #2 pair, subjected to either Gene Ontology – Biological Process (d) or KEGG Pathway
1160 analysis (e). Only the 10 categories with the largest enrichment ratios are shown. The color of
1161 each bar represents the false discovery rate (FDR) and the category names indicated in blue
1162 represent those linked to synapse formation and function or cell-cell communication. **(f.g)**
1163 Enrichment ratios observed in similar analyses conducted in d,e but with Gene-Set Enrichment
1164 Analysis (GSEA).

1165 **Figure 5: Enrichment of binding sites for splicing regulators NOVA1 and RBFOX1/2/3 in**
1166 **genes with altered splicing patterns in PTHS. (a)** Results from site enrichment analysis
1167 conducted on the sequences of skipped exons and neighboring introns for splicing events
1168 detected by rMATS-turbo in PTHS neurons, for RNA-binding proteins (RBP) NOVA1 and
1169 RBFOX1/2/3, with two motifs for NOVA1, one motif for RBFOX1 and one common motif for
1170 RBFOX2 and RBFOX3 (motif logos in the middle column). The statistical results from Fisher's
1171 exact test (*E*-value) in the comparison between the test dataset (sequences from splicing events
1172 in PTHS) and genomic sequences from a random set of genes are found in boldface text. For
1173 contrast, the *E*-values for the comparison between a positive control dataset (sequences of
1174 genes known to be regulated by the corresponding RBP) and the random control dataset are
1175 given in parentheses, and the *E*-values for the comparison between a negative control dataset
1176 (sequences of genes not known to be regulated by the corresponding RBP) and the random
1177 control dataset are given between <> symbols. **(b,c)** Examples of genomic sequence structure
1178 for two genes in our aberrant splicing dataset detected by rMATS-turbo, including the *SLC4A10*
1179 gene, shown to be enriched for NOVA1 binding sites (b) and the *CAMTA1* gene, shown to be
1180 enriched for RBFOX1/2/3 binding sites (c). The exons are shown as blue rectangles, connected
1181 by lines representing the introns. The binding sites are shown as black bars above the gene
1182 representation, and the chromosome numbers and genomic coordinate are also displayed. **(d)**
1183 Representation of NOVA1 and RBFOX1/2/3 binding sites in a random gene (MANBAL) not
1184 present in the aberrant splicing event list from PTHS neurons. **(e)** Violin plots representing the
1185 statistical comparison of the numbers of NOVA1 (left graph) and RBFOX1/2/3 (right graph)
1186 sites, in 100,000 nt, in the genes with the highest positive values of ∆PSI from the rMATS-turbo
1187 analysis of PTHS neurons (n=11 genes) compared with a random set of genes not present in
1188 the splicing event list in PTHS (n=12 genes). The median/interquartile range are shown as
1189 horizontal bars inside the violins. Welch's unpaired t-test assuming unequal variances; * $p<0.05$;
1190 ns, not statistically significantly different. **(f-h)** Venn diagrams representing the comparison
1191 between the number of genes with differential splicing events in PTHS neurons, as detected by
1192 rMATS-turbo in RNA-Seq data (absolute values of ∆PSI larger than 0.1), and the number of
1193 genes whose mRNA was shown in the literature to bind NOVA1 (f; ref [46]), NOVA1 (g; ref [63]), and
1194 RBFOX1 (h; ref [1]), in HITS-CliP experiments. The numbers of genes in each sector are shown
1195 inside the Venn diagrams, and some genes involved in neurodevelopment are highlighted in
1196 each intersection. Genes highlighted in blue are those present in the SFARI database of autism-
1197 related genes[78].

1198 **Figure 6: Aberrant splicing in Neurexin genes in PTHS. (a)** MA plot representing the
1199 differential splicing event prevalence, in the comparison between the PTHS patient-derived
1200 neurons and control neurons cultivated in vitro. The *x*-axis represents the expression
1201 abundance for each gene (represented as dots), in transcripts per million (TPM), while the *y*-
1202 axis shows the difference between the PSI (percent spliced in) for the patient cells and the
1203 control neurons (ΔPSI). Each dot represents a gene. Only a fraction of the genes is shown, to
1204 highlight the region of the graph where we observed a splicing event in the *NRXN2* gene
1205 chosen for further analysis. Blue dots indicate splicing events with a statistically significantly
1206 higher usage in control neurons, involving the number of genes displayed in parenthesis. The
1207 red dots indicate splicing events with higher usage in patient neurons. Gray dots are splicing
1208 events with a non-statistically significant difference in usage between patient and control cells.
1209 **(b)** Sashimi plots representing the splicing patterns for the NRXN2 splicing event highlighted in
1210 (a), depicting the location of exons 6, 7, and 8 in chromosome 11 (genomic coordinates below
1211 the plots). The vertical bars indicate the coverage of RNA-Seq reads in each exon or supporting
1212 the existence of each splice junction, in a *y*-axis scale shown as RPKM (reads per kilobase per
1213 million total reads). The cusp lines connecting the exons above or below the vertical bars
1214 indicate reads that support the existence of each corresponding exon-exon junction, with full
1215 lines representing junctions that include SE (skipped exon) 7, while dashed lines display
1216 functions that exclude said exon. The cusp thickness is proportional to the number of reads
1217 supporting the existence of each splice junction. The Sashimi plot on top (purple) represents the
1218 splicing pattern in control neurons, and the plot at the bottom (red) indicates the pattern in PTHS
1219 neurons, with the PSI values indicated above each graph. **(c)** Schematic representation of a
1220 fraction of the genomic sequence of NRXN2 gene, showing exons 6, 7, and 8. Three transcripts
1221 are shown: one represents the transcript that excludes exon 7 (SE-NRXN2-e), as detected by
1222 our rMATS-turbo analysis of PTHS neurons; the second represents the transcript including exon
1223 7 (SE-NRNX2-i), which also corresponds to a transcript in the Ensembl database (ENST entry
1224 number shown); the transcript at the bottom is another Ensembl transcript that includes a
1225 slightly longer version of exon 7. The amino acid translations for each transcript are shown
1226 below the DNA sequences. **(d)** Similar to (a), but for an event involving the *NRXN3* gene,
1227 chosen for further analyses. **(e)** Similar to (b), but for the event in (d), involving exons 20 and 21
1228 of the canonical transcript in the Ensembl database, and an additional exon not annotated in the
1229 canonical transcript (exon 20.5). **(f)** Similar to (c), showing two transcripts of the *NRXN3* gene,
1230 either including (SE-NRXN3-i) or excluding (SE-NRXN3-e) exon 20.5. **(g,h)** Genomic sequence
1231 structure for NRNX2 (g) and NRNX3 (h), showing the location of NOVA1 and RBFOX1/2/3

1232 binding sites. The exons are shown as blue rectangles (exon numbers below the gene
1233 structure), connected by lines representing the introns. The binding sites are shown as black
1234 bars above the gene representation, and the chromosome numbers and genomic coordinate
1235 are also displayed. The region containing the exons involved in the SE events are blown up
1236 below. The models at the bottom schematically depict the exons (to scale) and the splicing
1237 patterns in the SE-NRXN2/3-i and SE-NRXN2/3-e transcripts.

1238 **Figure 7: Changes in the abundances of transcript variants via exon skipping at the**
1239 **Neurexin-3 gene *NRXN3* in PTHS neurons in vitro. (a)** Schematic representation of the
1240 location of PCR primers in exons of the *NRXN3* gene, used in real-time qPCR experiments.
1241 Some oligos were designed to detect all transcript variants (left), because they detect a
1242 combination of exons present in both the transcript including (SE-NRXN3-i) and excluding (SE-
1243 NRXN3-e) exon 20.5. Other PCR oligos (right) were designed as variant-specific primers,
1244 because they recognize exon-exon splice junctions typical of either the SE-NRXN3-I or SE-
1245 NRXN3-e transcripts. **(b)** Real-time qPCR results showing the expression of *NRXN3* with the
1246 combination of oligos p1 and p2, which recognize both transcript variants. Each graph
1247 compares the expression in three patient lines (blue bars) and control line #1 (orange bar on the
1248 left graph) or control line #3 (orange bar on the right graph). Error bars are S.E.M. Each symbol
1249 represents a patient line, according to Supplementary Table S6. The expression is each graph
1250 is normalized to 1 in the control line, and the statistical comparisons (Welch's unpaired t-test
1251 assuming unequal variances) are between each patient line and the control shown in each
1252 graph. * $p<0.05$; ** $p<0.01$; ns, non-statistically significantly different. N=3 biological replicates
1253 per group. **(c)** Left: Bar plots representing the expression abundances of NRXN3 in control
1254 (orange) and PTHS (blue) neuronal cell lines, as judged by transcripts per million (TPM) in
1255 RNA-Seq data. Each symbol represents a patient or control. The control group has 3 subjects,
1256 while the PTHS group has 4 subjects; in three cases, the PTHS patient lines are matched with
1257 the corresponding parental control lines, and a fourth PTHS neuronal line is not matched to
1258 controls. Error bars are S.E.M. Notice the tendency for lower mean expression in the PTHS
1259 group, but the difference fell below the statistical significance threshold level, due to the low
1260 expression values in patient-parent pair #1 (circle symbols). Right: Direct comparison between
1261 the TPM expression abundances in three patient-parent pairs, represented as fold-change in
1262 the $\log_2$ scale. Error bars are S.E.M. **(d)** qPCR results with variant-specific oligos to detect the
1263 SE-NRXN3-e transcript (p1 and p3) or the SE-NRXN3-i (p4 and p5). The cell lines and
1264 comparisons are the same as in (c). Welch's unpaired t-test assuming unequal variances; *
1265 $p<0.05$; ** $p<0.01$. **(e)** Ratio between the relative expression of SE-NRXN3-i and SE-NRXN3-e
1266 transcript abundances, produced by contrasting the RQ (relative quantitation) levels with oligos
1267 p4+p5 with those obtained with primers p1+p3. In each graph, the mean ratio was normalized to
1268 1 in either control #1 (left) or control #3 (right) neuronal cell lines. N=3 independent biological
1269 replicates. Notice the change in the balance between the two transcript variants in two patient
1270 lines, with a reduction in the abundance of the transcript containing exon 20.5, as indicated by
1271 the mean ratio below 1 (dashed line). (f) Schematic representation of the location of primers for

1272 regular PCR amplification of specific *NRXN3* gene transcripts: oligos p6+p7 were designed to
1273 amplify just the SE-NRNX3-e variant, as p7 recognizes exon 21; oligos p6+p8 on the other hand
1274 were designed to amplify just the SE-NRNX3-i variant, as p8 recognizes the skipped exon 20.5
1275 (yellow). (g) Image of the results of gel electrophoresis showing amplification of several bands
1276 with the p6+p7 and p6+p8 primer combinations, with samples from patient line #2 and control
1277 line #1. L: Kasvi 1 kb DNA ladder. The open triangle indicates the 252-bp band expected from
1278 the SE-NRXN3-i transcript, while the filled triangle shows the 334-bp band expected from the
1279 SE-NRXN3-e transcript. Notice the almost complete absence of the band from the SE-NRXN3-i
1280 transcript in PTHS samples.

1281 **Figure 8: Evidence that the transcript variants of *NRXN3* encode transmembrane and**
1282 **secreted Neurexin-3 protein isoforms. (a)** Location of protein domains laminin G and EGF in
1283 the Neurexin-3 protein isoforms encoded by the SE-NRNX3-e and SE-NRNX3-i variants, as
1284 detected by InterProScan, showing the shorter length of the protein predicted to be produced
1285 from the variant included exon 20.5, due to the presence of a premature stop codon**. (b)**
1286 Schematic representation showing the coding sequences in transcripts SE-NRNX3-e and SE-
1287 NRNX3-i (hatched pattern), showing a detail of the premature stop codon introduced when exon
1288 20.5 is spliced into the transcript. Exon sizes are shown to scale, except for exon 21 in the
1289 bottom transcript, which is shown partially. **(c)** Prediction of protein topology using the
1290 DeepTMHMM tool on the proteins encoded by the SE-NRNX3-e (top) and SE-NRNX3-i (bottom)
1291 transcripts. The protein topology in each case is shown above the graph, color-coded according
1292 to the prediction of extracellular, intracellular, or transmembrane domains. The *y*-axis in the
1293 graph represents the probability of each portion of the protein being extracellular (orange),
1294 transmembrane (purple), or intracellular (blue). **(d)** Prediction of signal peptide and probability of
1295 secretion with the SignalP tool, on the first 70 amino acid residues in the protein sequences
1296 predicted from the SE-NRNX3-e and SE-NRNX3-i transcripts. Each line indicates the probability
1297 of the existence of a signal peptide (sigP) having features of N-terminal, central, or C-terminal
1298 portions of the signal peptide, while the dashed line is the remainder of the probability. **(e)**
1299 Western Blotting analysis of crude extracts from neuronal cultures in vitro, from patients #1 and
1300 #2, along with control #1. Three Neurexin bands are detected, including a ~50 kDa band (filled
1301 arrowhead) corresponding to the predicted molecular weight of Neurexin-β, as well as ~40 kDa
1302 bands (open arrowheads) with the predicted molecular weight of Neurexin-β lacking
1303 transmembrane domains. The endogenous control is GAPDH in all samples. The molecular
1304 weight markers shown on the left are from the PageRuler Unstained Protein Ladder (Thermo
1305 Fisher Scientific). **(f)** Similar to **e**, but with samples from cortical organoids. The graphs on the
1306 right show the quantitation of band intensity for the ~50 kDa and ~40 kDa bands, as well as the
1307 ratio between both bands, normalized against the control #1 sample. Notice the nearly absent
1308 expression of one of the ~40 kDa Neurexin-β bands, whose intensity decreases more
1309 prominently than the ~50 kDa band.

Figure 1

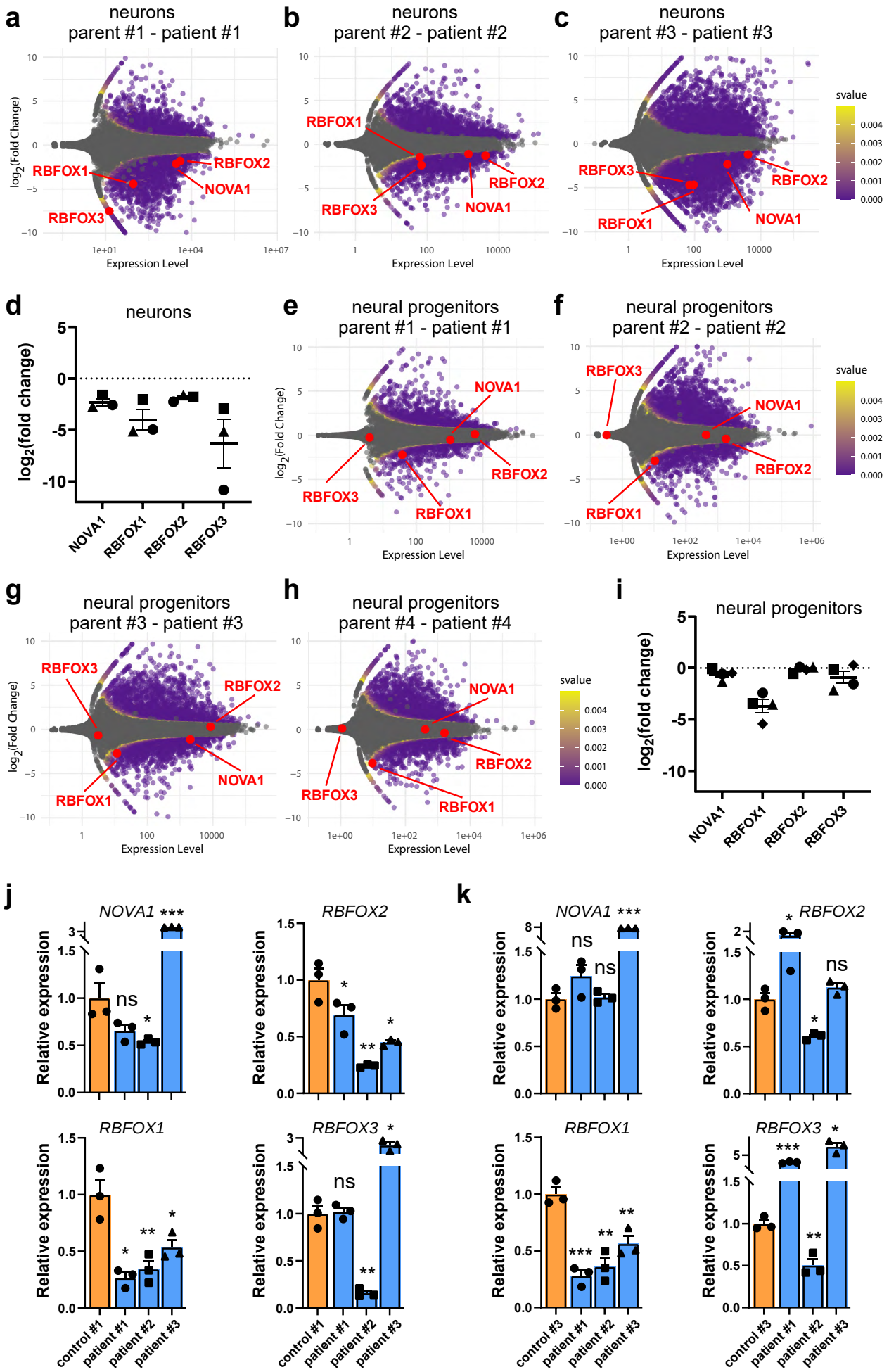
a
neurons
parent #1 - patient #1
b
neurons
parent #2 - patient #2
c
neurons
parent #3 - patient #3
svalue
0.004
0.003
0.002
0.001
0.000
log2(Fold Change)
Expression Level
RBFOX1
RBFOX2
RBFOX3
NOVA1
d
neurons
log2(fold change)
NOVA1
RBFOX1
RBFOX2
RBFOX3
e
neural progenitors
parent #1 - patient #1
f
neural progenitors
parent #2 - patient #2
g
neural progenitors
parent #3 - patient #3
h
neural progenitors
parent #4 - patient #4
i
neural progenitors
j
NOVA1 ***
RBFOX2
RBFOX1
RBFOX3 *
Relative expression
ns
control #1
patient #1
patient #2
patient #3
k
NOVA1 ***
RBFOX2
RBFOX1
RBFOX3 *
control #3
patient #1
patient #2
patient #3

Figure 2

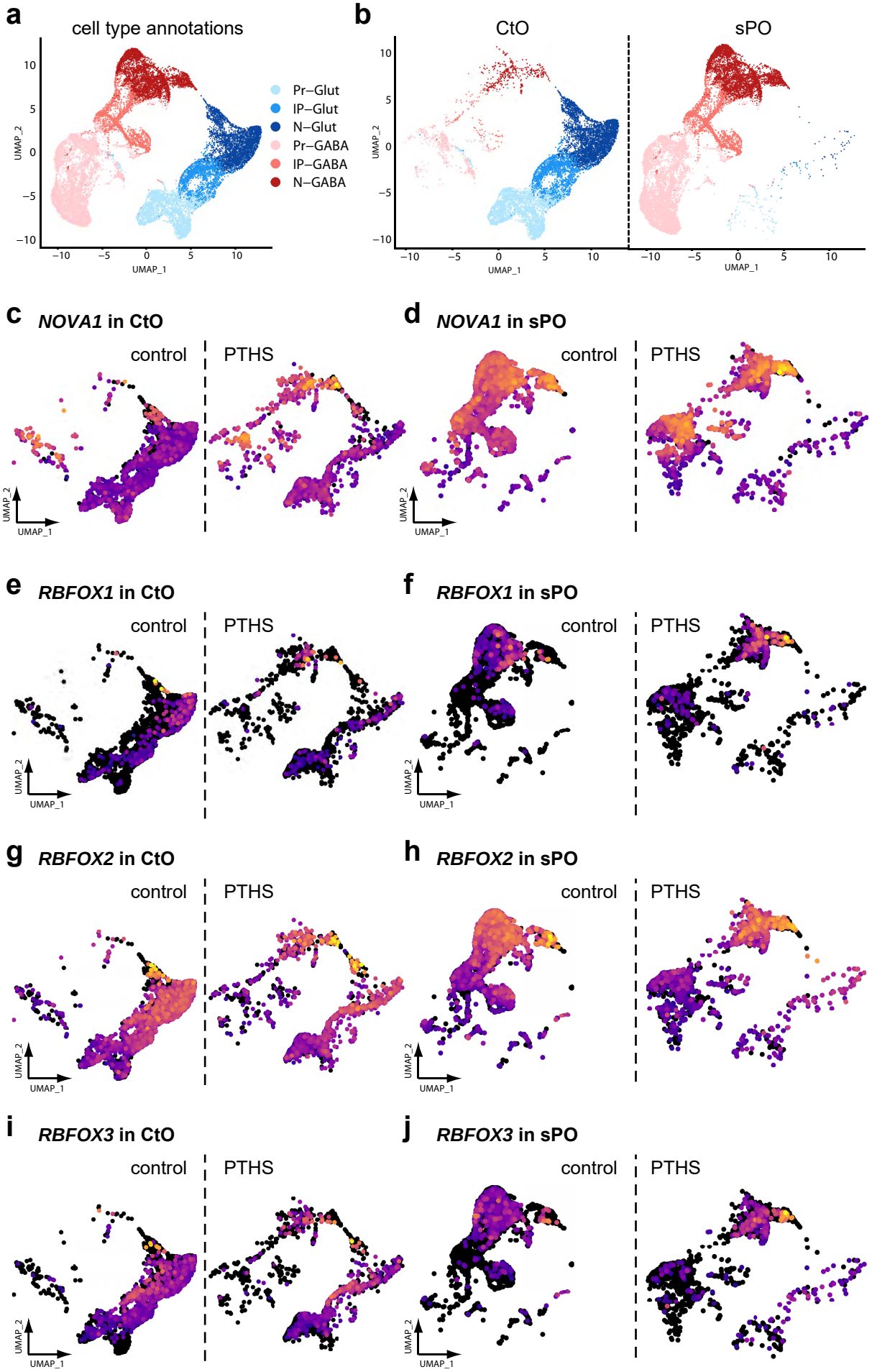
a
cell type annotations
Pr–Glut
IP–Glut
N–Glut
Pr–GABA
IP–GABA
N–GABA
UMAP_1
UMAP_2
b
CtO
sPO
c NOVA1 in CtO
control
PTHS
d NOVA1 in sPO
e RBFOX1 in CtO
f RBFOX1 in sPO
g RBFOX2 in CtO
h RBFOX2 in sPO
i RBFOX3 in CtO
j RBFOX3 in sPO

Figure 3

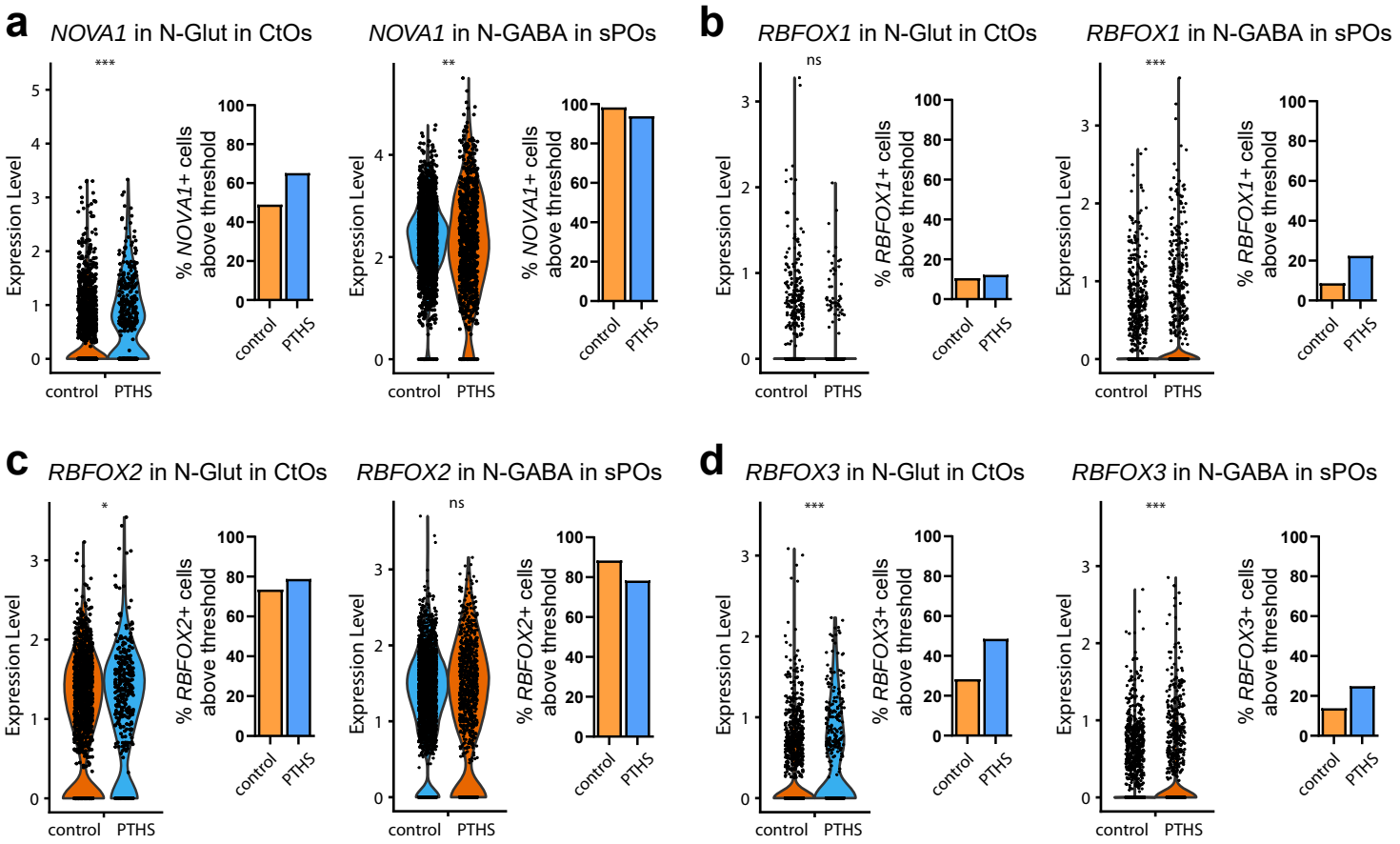
a
NOVA1 in N-Glut in CtOs
NOVA1 in N-GABA in sPOs
b
RBFOX1 in N-Glut in CtOs
RBFOX1 in N-GABA in sPOs
c
RBFOX2 in N-Glut in CtOs
RBFOX2 in N-GABA in sPOs
d
RBFOX3 in N-Glut in CtOs
RBFOX3 in N-GABA in sPOs
Expression Level
% NOVA1+ cells above threshold
% RBFOX1+ cells above threshold
% RBFOX2+ cells above threshold
% RBFOX3+ cells above threshold
control
PTHS
***
**
ns
*

Figure 4

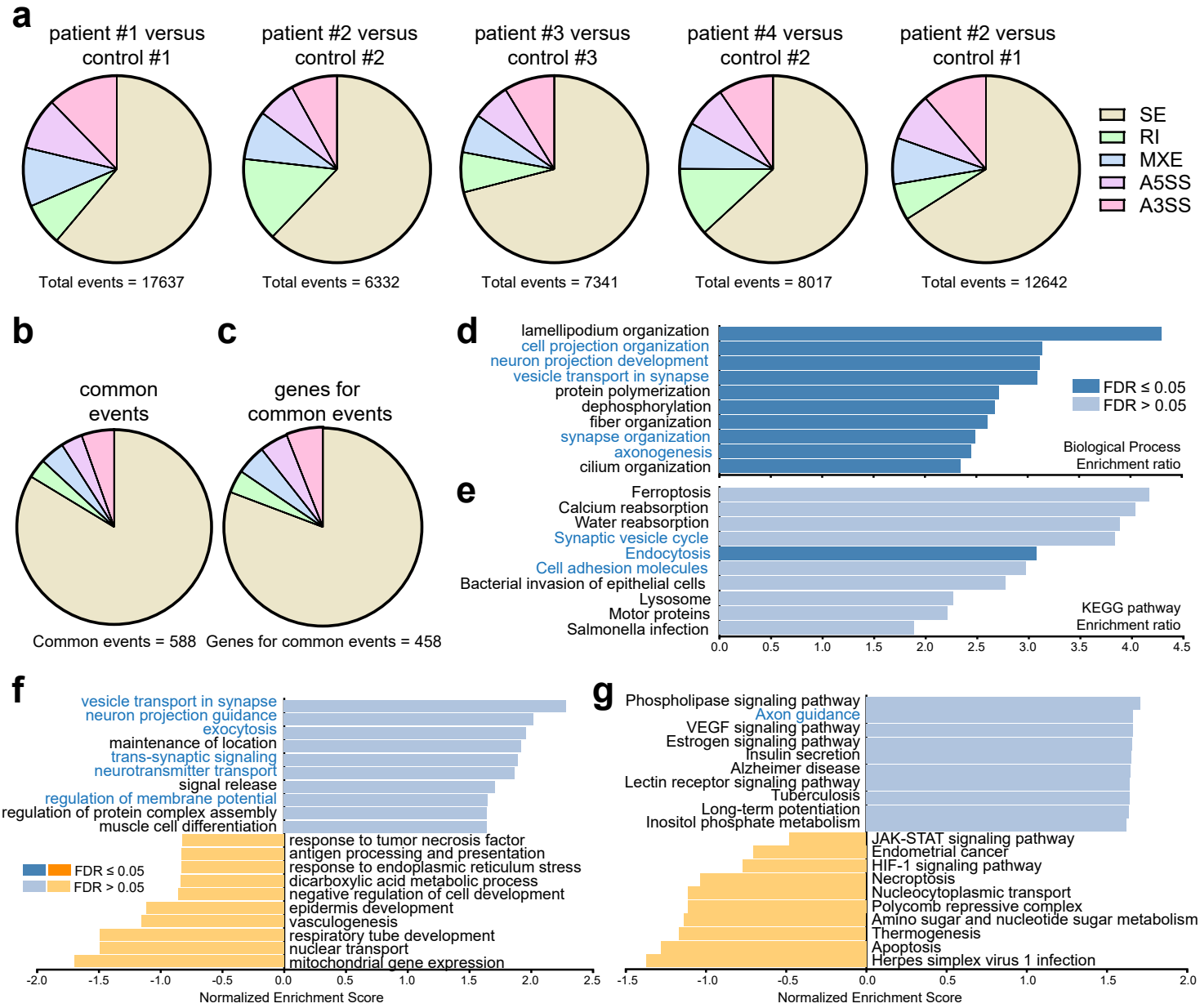
a
patient #1 versus control #1
patient #2 versus control #2
patient #3 versus control #3
patient #4 versus control #2
patient #2 versus control #1
SE
RI
MXE
A5SS
A3SS
Total events = 17637
Total events = 6332
Total events = 7341
Total events = 8017
Total events = 12642
b
common events
Common events = 588
c
genes for common events
Genes for common events = 458
d
lamellipodium organization
cell projection organization
neuron projection development
vesicle transport in synapse
protein polymerization
dephosphorylation
fiber organization
synapse organization
axonogenesis
cilium organization
FDR ≤ 0.05
FDR > 0.05
Biological Process
Enrichment ratio
e
Ferroptosis
Calcium reabsorption
Water reabsorption
Synaptic vesicle cycle
Endocytosis
Cell adhesion molecules
Bacterial invasion of epithelial cells
Lysosome
Motor proteins
Salmonella infection
KEGG pathway
Enrichment ratio
0.0 0.5 1.0 1.5 2.0 2.5 3.0 3.5 4.0 4.5
f
vesicle transport in synapse
neuron projection guidance
exocytosis
maintenance of location
trans-synaptic signaling
neurotransmitter transport
signal release
regulation of membrane potential
regulation of protein complex assembly
muscle cell differentiation
response to tumor necrosis factor
antigen processing and presentation
response to endoplasmic reticulum stress
dicarboxylic acid metabolic process
negative regulation of cell development
epidermis development
vasculogenesis
respiratory tube development
nuclear transport
mitochondrial gene expression
FDR ≤ 0.05
FDR > 0.05
-2.0 -1.5 -1.0 -0.5 0.0 0.5 1.0 1.5 2.0 2.5
Normalized Enrichment Score
g
Phospholipase signaling pathway
Axon guidance
VEGF signaling pathway
Estrogen signaling pathway
Insulin secretion
Alzheimer disease
Lectin receptor signaling pathway
Tuberculosis
Long-term potentiation
Inositol phosphate metabolism
JAK-STAT signaling pathway
Endometrial cancer
HIF-1 signaling pathway
Necroptosis
Nucleocytoplasmic transport
Polycomb repressive complex
Amino sugar and nucleotide sugar metabolism
Thermogenesis
Apoptosis
Herpes simplex virus 1 infection
-1.5 -1.0 -0.5 0.0 0.5 1.0 1.5 2.0
Normalized Enrichment Score

Figure 5

a

RBP	motif logo	site enrichment *E*-value test against random set (pos. ctrl against random set) <neg. ctrl against random set>
NOVA1 motif #1		**9.2 x E-08** (2.9 x E-01) <2.2 x E-00>
NOVA1 motif #2		**3.0 x E-08** (1.6 x E-06) <5.9 x E-01>
RBFOX1		**5.8 x E-04** (8.4 x E-08) <3.2 x E-00>
RBFOX2/3		**4.1 x E-07** (9.2 x E-16) <2.4 x E-00>

b

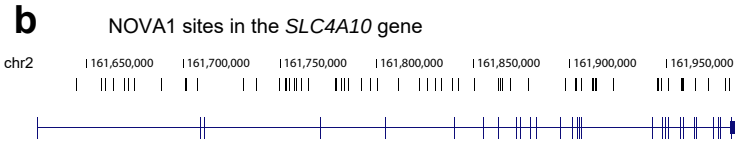

c

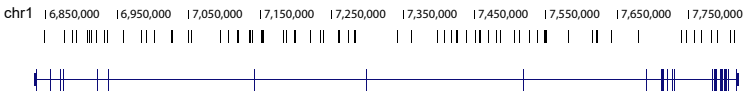

d

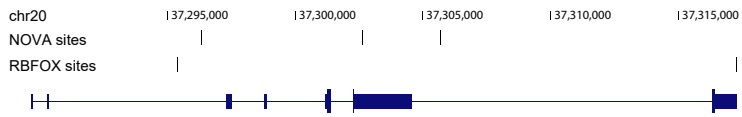

e

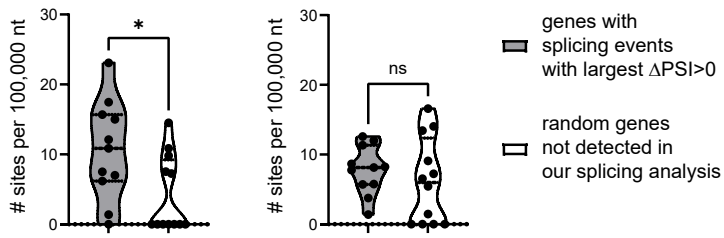

f

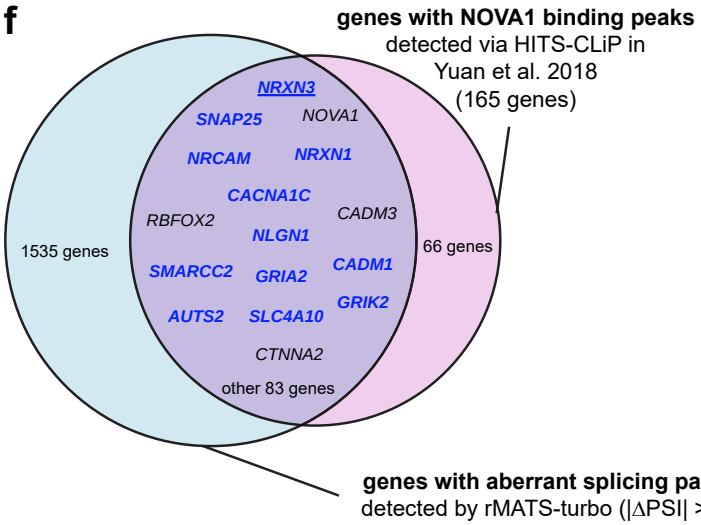

g

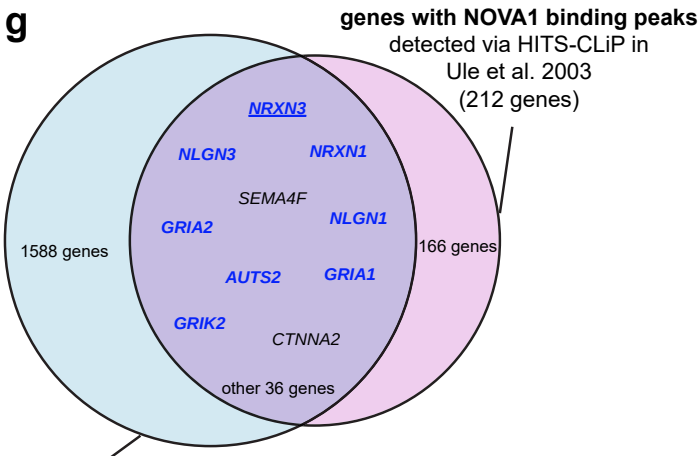

genes with aberrant splicing pattern detected by rMATS-turbo (|ΔPSI| > 0.1) (1634 genes)

h

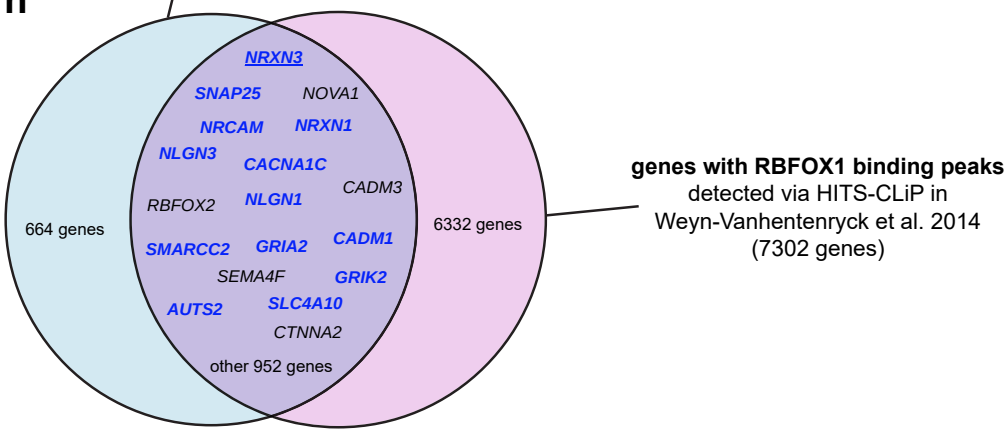

Figure 6

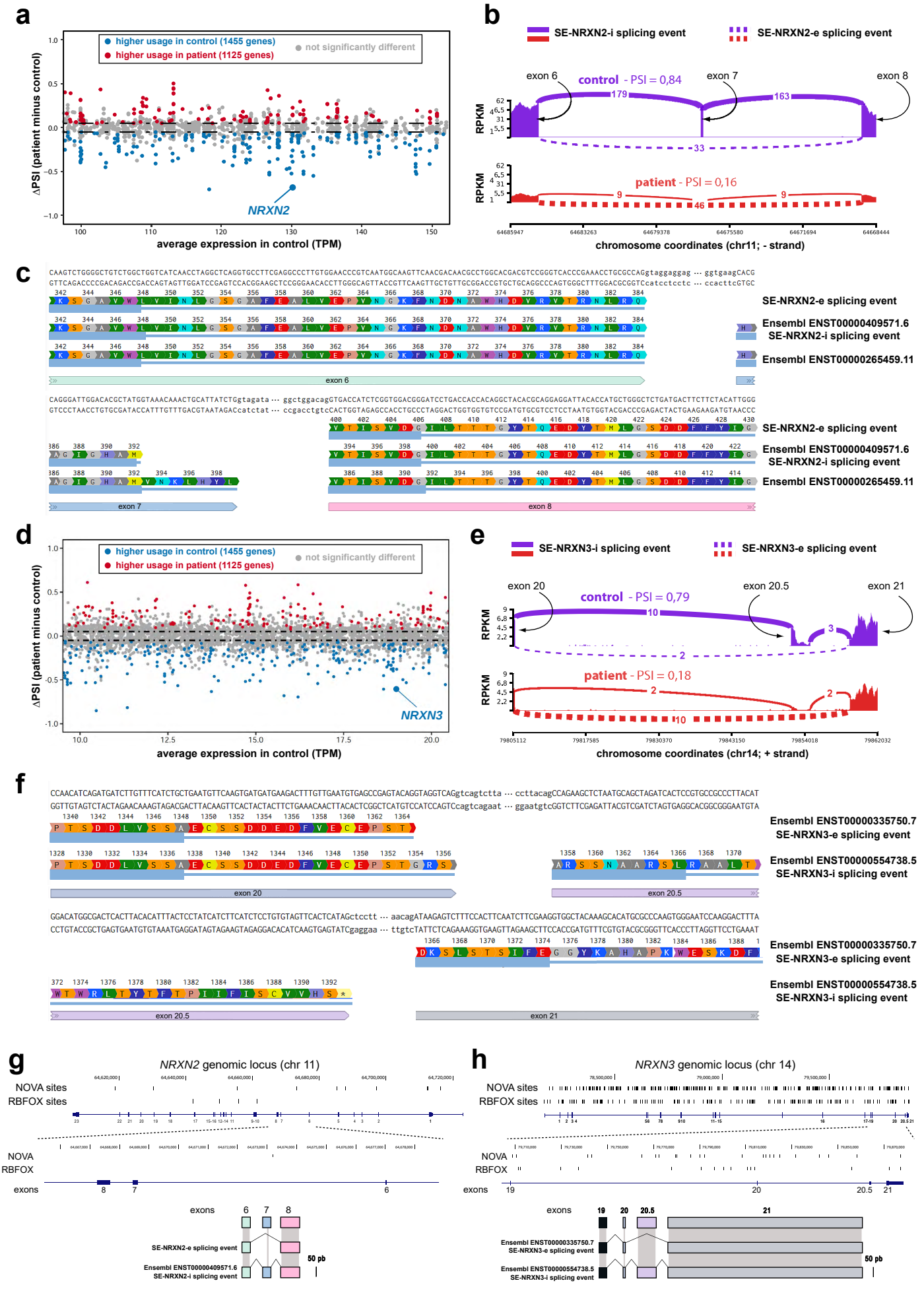
a
higher usage in control (1455 genes)
higher usage in patient (1125 genes)
not significantly different
ΔPSI (patient minus control)
NRXN2
average expression in control (TPM)
b
SE-NRXN2-i splicing event
SE-NRXN2-e splicing event
exon 6
control - PSI = 0,84
exon 7
exon 8
RPKM
patient - PSI = 0,16
chromosome coordinates (chr11; - strand)
c
SE-NRXN2-e splicing event
Ensembl ENST00000409571.6
SE-NRXN2-i splicing event
Ensembl ENST00000265459.11
exon 6
exon 7
exon 8
d
higher usage in control (1455 genes)
higher usage in patient (1125 genes)
not significantly different
ΔPSI (patient minus control)
NRXN3
average expression in control (TPM)
e
SE-NRXN3-i splicing event
SE-NRXN3-e splicing event
exon 20
control - PSI = 0,79
exon 20.5
exon 21
RPKM
patient - PSI = 0,18
chromosome coordinates (chr14; + strand)
f
Ensembl ENST00000335750.7
SE-NRXN3-e splicing event
Ensembl ENST00000554738.5
SE-NRXN3-i splicing event
exon 20
exon 20.5
exon 21
g
NRXN2 genomic locus (chr 11)
NOVA sites
RBFOX sites
NOVA
RBFOX
exons
SE-NRXN2-e splicing event
Ensembl ENST00000409571.6
SE-NRXN2-i splicing event
50 pb
h
NRXN3 genomic locus (chr 14)
NOVA sites
RBFOX sites
NOVA
RBFOX
exons
Ensembl ENST00000335750.7
SE-NRXN3-e splicing event
Ensembl ENST00000554738.5
SE-NRXN3-i splicing event
50 pb

Figure 7

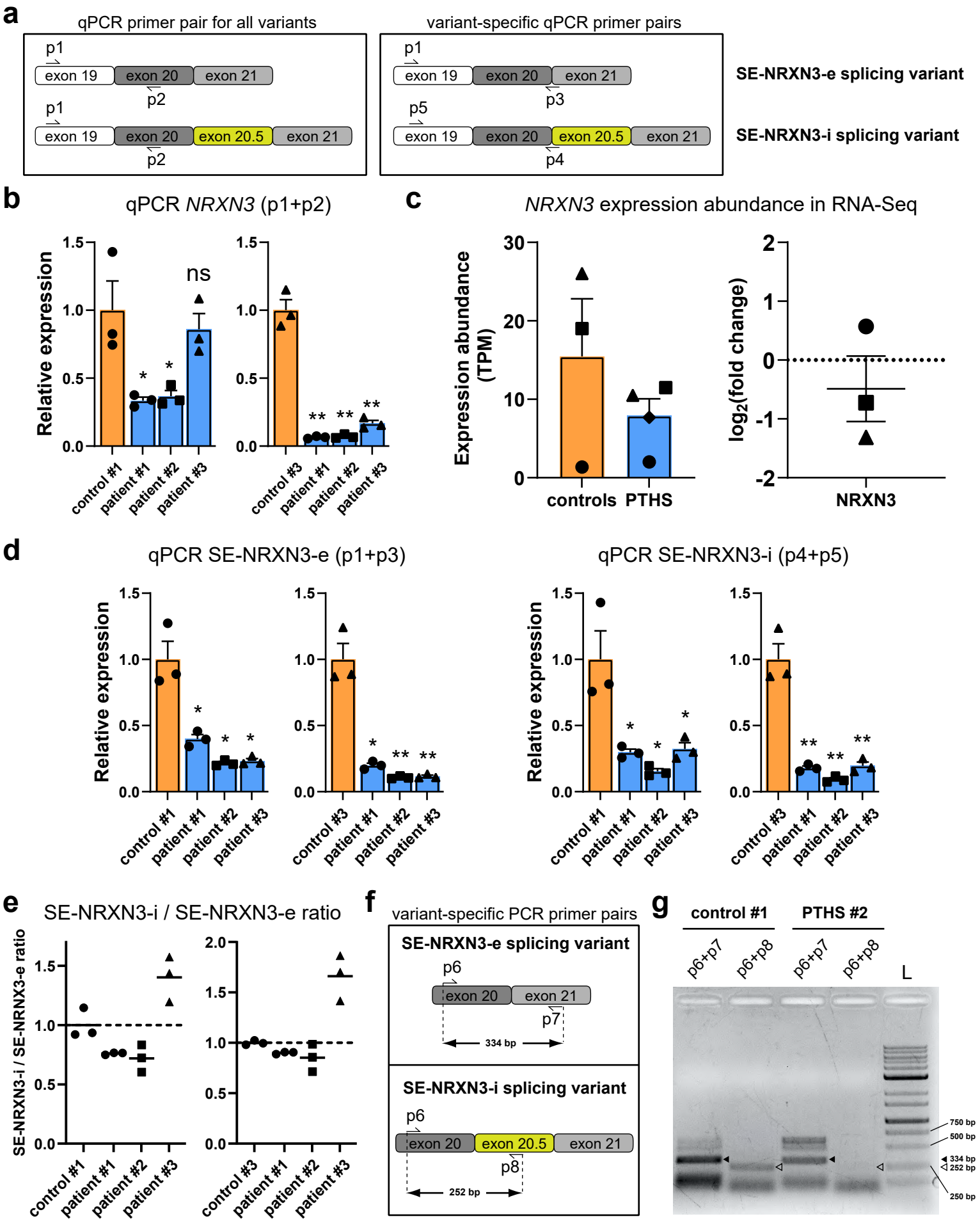
a
qPCR primer pair for all variants
variant-specific qPCR primer pairs
p1
exon 19
exon 20
exon 21
p2
exon 20.5
p5
p3
p4
SE-NRXN3-e splicing variant
SE-NRXN3-i splicing variant
b
qPCR NRXN3 (p1+p2)
Relative expression
ns
control #1
patient #1
patient #2
patient #3
control #3
c
NRXN3 expression abundance in RNA-Seq
Expression abundance (TPM)
controls
PTHS
log2(fold change)
NRXN3
d
qPCR SE-NRXN3-e (p1+p3)
qPCR SE-NRXN3-i (p4+p5)
e
SE-NRXN3-i / SE-NRXN3-e ratio
f
variant-specific PCR primer pairs
SE-NRXN3-e splicing variant
p6
p7
334 bp
SE-NRXN3-i splicing variant
p8
252 bp
g
control #1
PTHS #2
p6+p7
p6+p8
L
750 bp
500 bp
334 bp
252 bp
250 bp

Figure 8

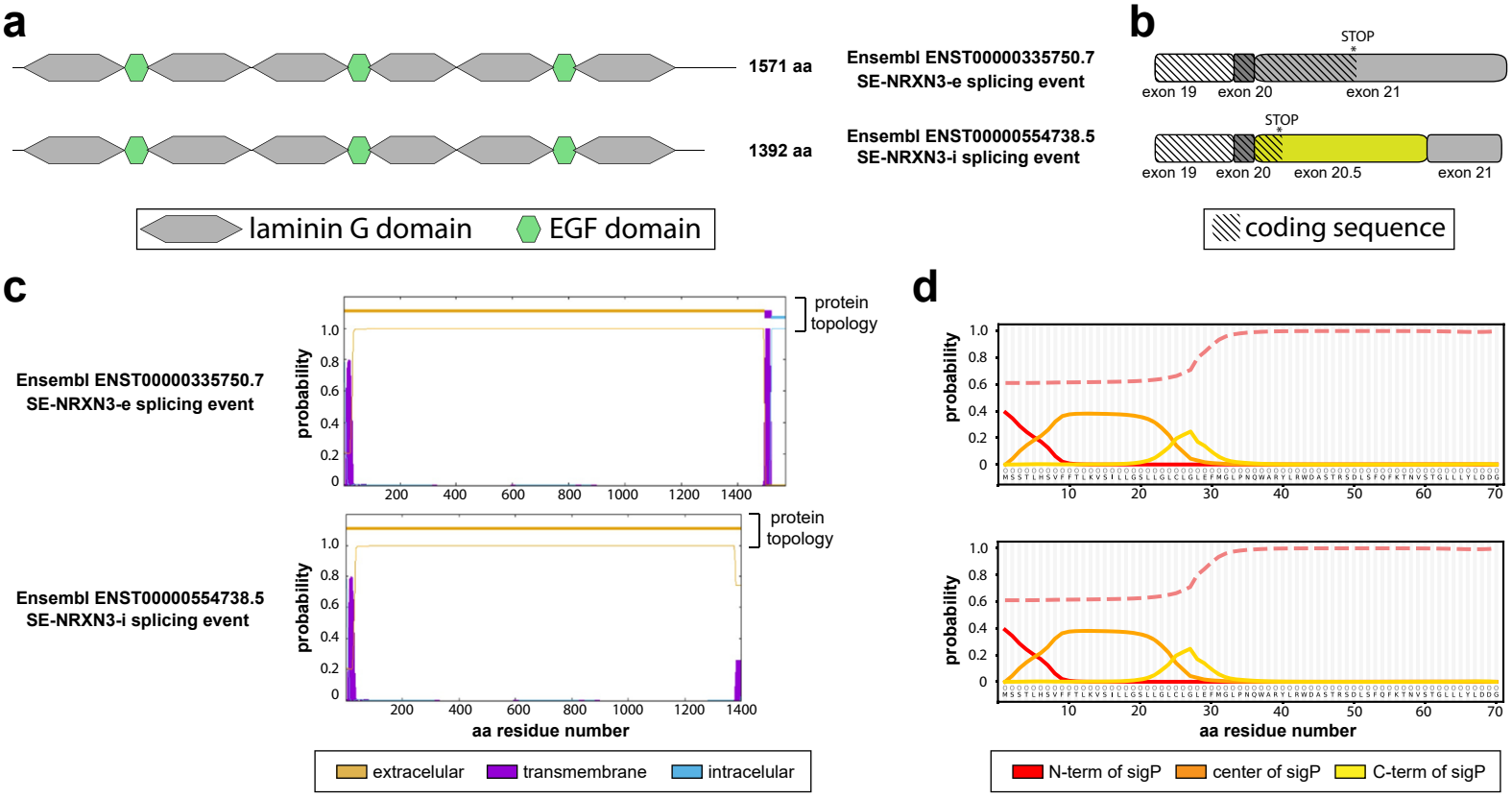
a
1571 aa
Ensembl ENST00000335750.7
SE-NRXN3-e splicing event
1392 aa
Ensembl ENST00000554738.5
SE-NRXN3-i splicing event
laminin G domain
EGF domain
b
STOP
exon 19
exon 20
exon 21
STOP
exon 19
exon 20
exon 20.5
exon 21
coding sequence
c
Ensembl ENST00000335750.7
SE-NRXN3-e splicing event
Ensembl ENST00000554738.5
SE-NRXN3-i splicing event
probability
protein topology
aa residue number
extracelular
transmembrane
intracelular
d
probability
aa residue number
N-term of sigP
center of sigP
C-term of sigP

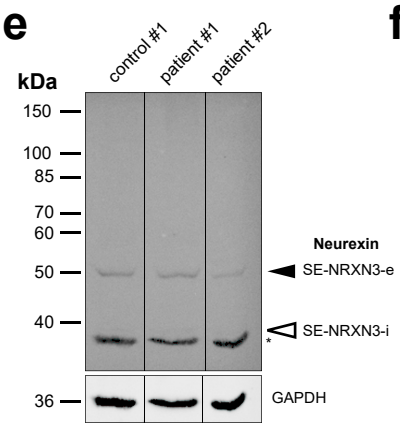
e
control #1
patient #1
patient #2
kDa
150
100
85
70
60
50
40
36
Neurexin
SE-NRXN3-e
SE-NRXN3-i
GAPDH

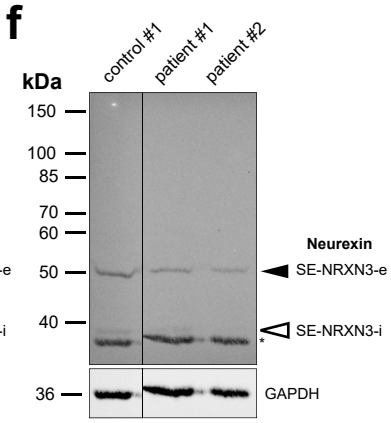
f
control #1
patient #1
patient #2
kDa
150
100
85
70
60
50
40
36
Neurexin
SE-NRXN3-e
SE-NRXN3-i
GAPDH

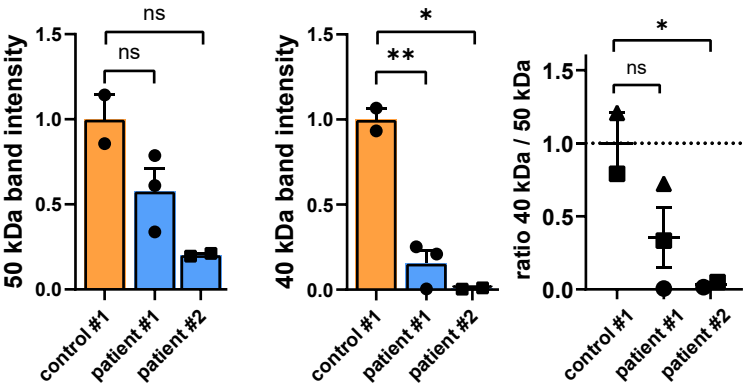
50 kDa band intensity
40 kDa band intensity
ratio 40 kDa / 50 kDa
ns
*
**
control #1
patient #1
patient #2

Supplementary Material

Supplementary Figure Legends

Supplementary Figure S1: Over-representation analysis of genes involved in splicing events differentially used in PTHS. Enrichment ratios observed in Over-Representation Analysis (ORA) of splicing events with an absolute value of DPSI larger than 0.3 in the patient-control #2 pair, subjected to either Gene Ontology – Biological Process (top in each panel) or KEGG Pathway analysis (bottom in each panel). Only the 10 categories with the largest enrichment ratios are shown. The color of each bar represents the false discovery rate (FDR) and the category names indicated in blue represent those linked to synapse formation and function or cell-cell communication. The patient-control pairs shown in this figure complement the data for pair #2 presented in Fig. 4d,e.

Supplementary Figure S2: Gene-set enrichment analysis of genes involved in splicing events differentially used in PTHS. Enrichment ratios observed in Gene-Set Enrichment Analysis (GSEA) of splicing events with an absolute value of DPSI larger than 0.3 in the patient-control #2 pair, subjected to either Gene Ontology – Biological Process (left in each group) or KEGG Pathway analysis (right in each group). Only the 10 categories with the largest enrichment ratios are shown. The color of each bar represents the false discovery rate (FDR) and the category names indicated in blue represent those linked to synapse formation and function or cell-cell communication. The patient-control pairs shown in this figure complement the data for pair #2 presented in Fig. 4f,g.

Supplementary Figure S3: Supporting data for the analysis of splicing patterns in the *NRXN3* gene via PCR and Sanger sequencing. (a) Structure of the *NRNX3* (Neurexin-3) genomic locus, with the distribution of exons. Notice that exon 20.5 is annotated as an additional exon between 20 and 21, because it is not part of the transcript exhibited as the canonical *NRXN3* transcript in Ensembl. **(b)** Schematic representation of the coding exons in the *NRXN3* gene, with the location of PCR oligos to amplify the exon-exon junctions: primers p6 and p7 amplify the transcript variant without exon 20.5 (SE-NRXN3-e), while primers p6 and p8 amplify the transcript variant including exon 20.5 (SE-NRXN3-i). Exons are shown to scale. **(c)** Representation of the primer combinations and expected amplicon sizes, as well as an example of amplicon sequence. The frequencies of each amplicon in control and PTHS samples are shown in the last two columns (numbers in parentheses represent the total number of amplicons sequenced).

Supplementary Table Legends

Supplementary Table S1: Expression abundances of selected genes in RNA-Seq data from PTHS and control neurons and neural progenitor cells. The expression abundances in independent biological replicates (A, B, and C) for each subject, in transcripts per million reads (TPM), are shown for a selection of splicing regulators in the NOVA and RBFOX families. The means of expression in each subjects and log fold-changes (in base 2) for the comparison between each subject and a control are also shown.

Supplementary Table S2: Splicing pattern analysis results using rMATS-turbo. Each tab contains the filtered rMATS-turbo output for one patient versus control pair. Different tabs also indicate the results for the five types of alternative splicing: skipped exon (SE), alternative 5′ splice site (A5SS), alternative 3′ splice site (A3SS), mutually exclusive exon (MXE), and retained intron (RI). The common columns in all tabs are as follows: “ID”: rMATS event ID; “GeneID”: Ensembl gene ID; “geneSymbol”: gene name; “chr”: chromosome; “strand”: strand of the gene; “IJC_SAMPLE_1”: number of counts that support the inclusion of the splicing event, for the control sample (replicates are comma-separated); “SJC_SAMPLE_1”: number of counts that support the exclusion of the splicing event, for the control sample (replicates are comma-separated); “IJC_SAMPLE_2”: number of counts that support the inclusion of the splicing event, for the patien sample (replicates are comma-separated); “SJC_SAMPLE_2”: number of counts that support the exclusion of the splicing event, for the patient sample (replicates are comma-separated); “IncFormLen”: length of inclusion form, used for normalization purposes; “SkipFormLen”: length of skipping form, used for normalization purposes; “PValue”: significance of splicing difference between the two sample groups; “FDR”: false discovery rate; “IncLevel1”: inclusion level (in percentage) for the control sample (replicates are comma-separated), calculated from normalized counts; “IncLevel2”: inclusion level (in percentage) for the patient sample (replicates are comma-separated), calculated from normalized counts; “IncLevelDifference”: average(IncLevel1) − average(IncLevel2). See also the meaning of other columns, which indicate the genomic coordinates of the exons involved, in the rMATS-turbo original publication[1].

Supplementary Table S3: Common splicing events (and respective genes) detected by rMATS-turbo across all patient-control pairs. Each of the first 5 tabs lists the common splicing events in each of the five categories of alternative splicing (SE, RI, MXE, A5SS, and A3SS). The meaning of each column is the same as in Supplementary Table S2. The last 5 tabs list the genes corresponding to these common splicing events.

Supplementary Table S4: List of genes known to be regulated by NOVA1 and RBFOX1/2/3 splicing regulators. Each tab lists the genes for which we extracted genomic sequences to produce the positive control datasets used for the Site Enrichment Analysis (SEA), for NOVA1 and RBFOX1/2/3. In the latter case, we combined information pertaining to genes known to be regulated by RBFOX1, RBFOX2, and/or RBFOX3 into a single list.

Supplementary Table S5: Lists of genes detected by rMATS-turbo in our PTHS splicing analysis and lists of genes binding NOVA and RBFOX splicing regulators. The first tab lists the genes for which our rMATS-turbo analysis detected aberrant splicing events, using a threshold of absolute values of ΔPSI above 0.1. The last three tabs contain lists of genes detected by HITS-CLiP in published datasets, focusing on NOVA1[2,3] or RBFOX1/2/3[4]. These lists were used to produce the Venn diagrams in Fig 5f-h.

Supplementary Table S6: Summary of participating subjects and clinical characteristics. For all patients, controls are parents of matching sex. Abbreviations: FG: dysmorphic facial *gestalt*; SM/MM: severe (SM) or mild (MM) motor delay at age 3; AS: absent speech; CT: constipation; SZ: seizures; BA: breathing problems (hyperventilation or apnea); UA: urinary abnormalities (retention or incontinence); VA: visual abnormalities (ocular anomalies); RB: repetitive behaviors; abMRI: brain anomalies (thinned *corpus callosum*) detected by MRI.

Supplementary Table S7: Motifs for NOVA1 and RBFOX1/2/3 used for motif search and enrichment analyses. The RBP motifs for NOVA1, RBFOX1, RBFOX2, and RBFOX3 are shown in tabular PSSM (Position-Specific Scoring Matrix) format.

Supplementary Table S8: Summary of statistical tests and metrics. For all figure panels (listed in order of appearance in the paper), we present complete statistical evaluation results, including type of analysis, groups being compared, means and standard errors of the means (SEM) for each group, numbers of subjects, independent replicates, technical replicates, or numbers of cells, as well as the number of observations used to calculate means and perform statistical comparisons (N), the statistical test used, metrics results (t, H, W, or F), effect sizes, exact p-values for global statistical comparisons, and, when necessary, effect sizes and exact p-values for each individual pairwise comparison after post-hoc test. When experimentation involved more than one independent replicate per subject cell line, or more than one technical replicate per independent biological replicate, these numbers are also indicated in separate columns, even though the statistical test was computed based solely on the means of different lines in these cases. The comparisons of gene expression between control and PTHS single cell RNA-Seq libraries are listed in the second tab (part 2), including gene name, cell types, groups being compared, means and SEM, fold change (PTHS versus control), as well as statistical test results.

Supplementary Material References

1. Wang, Y. *et al.* rMATS-turbo: an efficient and flexible computational tool for alternative splicing analysis of large-scale RNA-seq data. *Nature Protocols 2024 19:4* 19, 1083–1104 (2024).

2. Yuan, Y. *et al.* Cell type-specific CLIP reveals that NOVA regulates cytoskeleton interactions in motoneurons. *Genome Biol* 19, 1–19 (2018).

3. Ule, J. *et al.* CLIP identifies Nova-regulated RNA networks in the brain. *Science* 302, 1212–1215 (2003).

4. Weyn-Vanhentenryck, S. M. *et al.* HITS-CLIP and Integrative Modeling Define the Rbfox Splicing-Regulatory Network Linked to Brain Development and Autism. *Cell Rep* 6, 1139–1152 (2014).

Figure S1

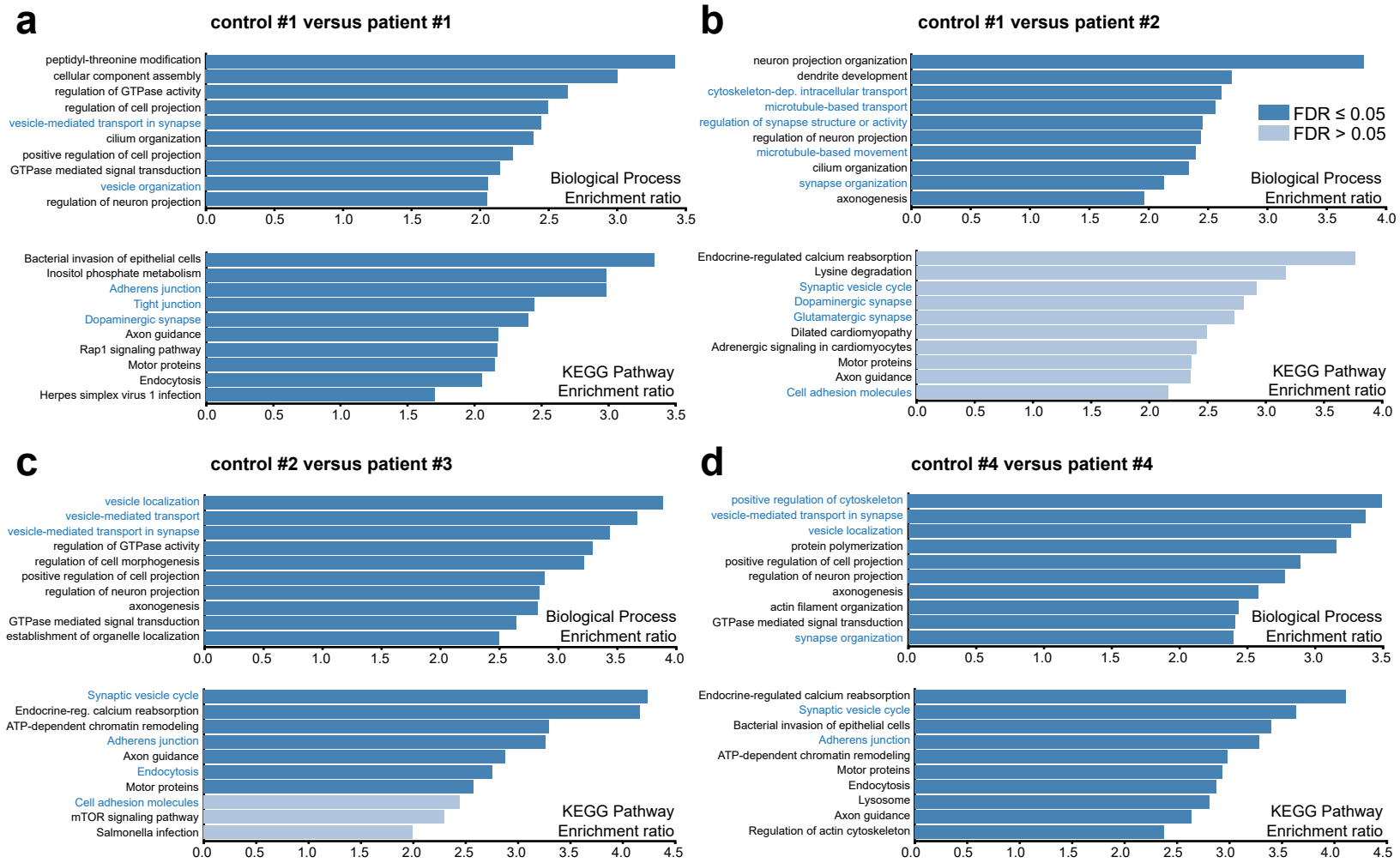
a
control #1 versus patient #1
peptidyl-threonine modification
cellular component assembly
regulation of GTPase activity
regulation of cell projection
vesicle-mediated transport in synapse
cilium organization
positive regulation of cell projection
GTPase mediated signal transduction
vesicle organization
regulation of neuron projection
Biological Process
Enrichment ratio
0.0 0.5 1.0 1.5 2.0 2.5 3.0 3.5
Bacterial invasion of epithelial cells
Inositol phosphate metabolism
Adherens junction
Tight junction
Dopaminergic synapse
Axon guidance
Rap1 signaling pathway
Motor proteins
Endocytosis
Herpes simplex virus 1 infection
KEGG Pathway
Enrichment ratio
0.0 0.5 1.0 1.5 2.0 2.5 3.0 3.5
b
control #1 versus patient #2
neuron projection organization
dendrite development
cytoskeleton-dep. intracellular transport
microtubule-based transport
regulation of synapse structure or activity
regulation of neuron projection
microtubule-based movement
cilium organization
synapse organization
axonogenesis
FDR ≤ 0.05
FDR > 0.05
Biological Process
Enrichment ratio
0.0 0.5 1.0 1.5 2.0 2.5 3.0 3.5 4.0
Endocrine-regulated calcium reabsorption
Lysine degradation
Synaptic vesicle cycle
Dopaminergic synapse
Glutamatergic synapse
Dilated cardiomyopathy
Adrenergic signaling in cardiomyocytes
Motor proteins
Axon guidance
Cell adhesion molecules
KEGG Pathway
Enrichment ratio
0.0 0.5 1.0 1.5 2.0 2.5 3.0 3.5 4.0
c
control #2 versus patient #3
vesicle localization
vesicle-mediated transport
vesicle-mediated transport in synapse
regulation of GTPase activity
regulation of cell morphogenesis
positive regulation of cell projection
regulation of neuron projection
axonogenesis
GTPase mediated signal transduction
establishment of organelle localization
Biological Process
Enrichment ratio
0.0 0.5 1.0 1.5 2.0 2.5 3.0 3.5 4.0
Synaptic vesicle cycle
Endocrine-reg. calcium reabsorption
ATP-dependent chromatin remodeling
Adherens junction
Axon guidance
Endocytosis
Motor proteins
Cell adhesion molecules
mTOR signaling pathway
Salmonella infection
KEGG Pathway
Enrichment ratio
0.0 0.5 1.0 1.5 2.0 2.5 3.0 3.5 4.0 4.5
d
control #4 versus patient #4
positive regulation of cytoskeleton
vesicle-mediated transport in synapse
vesicle localization
protein polymerization
positive regulation of cell projection
regulation of neuron projection
axonogenesis
actin filament organization
GTPase mediated signal transduction
synapse organization
Biological Process
Enrichment ratio
0.0 0.5 1.0 1.5 2.0 2.5 3.0 3.5
Endocrine-regulated calcium reabsorption
Synaptic vesicle cycle
Bacterial invasion of epithelial cells
Adherens junction
ATP-dependent chromatin remodeling
Motor proteins
Endocytosis
Lysosome
Axon guidance
Regulation of actin cytoskeleton
KEGG Pathway
Enrichment ratio
0.0 0.5 1.0 1.5 2.0 2.5 3.0 3.5 4.0 4.5

Figure S2

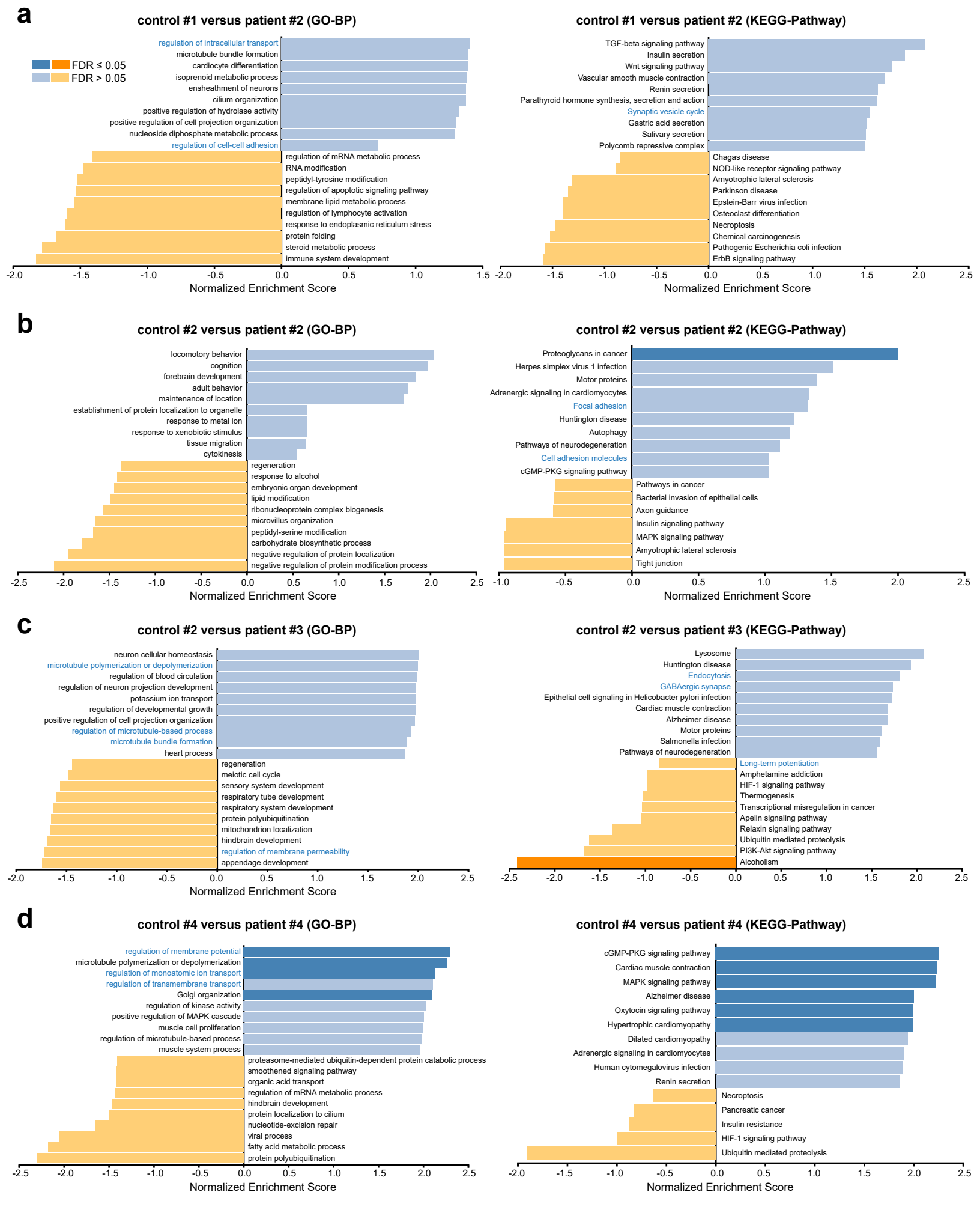
a
control #1 versus patient #2 (GO-BP)
FDR ≤ 0.05
FDR > 0.05
regulation of intracellular transport
microtubule bundle formation
cardiocyte differentiation
isoprenoid metabolic process
ensheathment of neurons
cilium organization
positive regulation of hydrolase activity
positive regulation of cell projection organization
nucleoside diphosphate metabolic process
regulation of cell-cell adhesion
regulation of mRNA metabolic process
RNA modification
peptidyl-tyrosine modification
regulation of apoptotic signaling pathway
membrane lipid metabolic process
regulation of lymphocyte activation
response to endoplasmic reticulum stress
protein folding
steroid metabolic process
immune system development
-2.0 -1.5 -1.0 -0.5 0.0 0.5 1.0 1.5
Normalized Enrichment Score
control #1 versus patient #2 (KEGG-Pathway)
TGF-beta signaling pathway
Insulin secretion
Wnt signaling pathway
Vascular smooth muscle contraction
Renin secretion
Parathyroid hormone synthesis, secretion and action
Synaptic vesicle cycle
Gastric acid secretion
Salivary secretion
Polycomb repressive complex
Chagas disease
NOD-like receptor signaling pathway
Amyotrophic lateral sclerosis
Parkinson disease
Epstein-Barr virus infection
Osteoclast differentiation
Necroptosis
Chemical carcinogenesis
Pathogenic Escherichia coli infection
ErbB signaling pathway
-2.0 -1.5 -1.0 -0.5 0.0 0.5 1.0 1.5 2.0 2.5
Normalized Enrichment Score
b
control #2 versus patient #2 (GO-BP)
locomotory behavior
cognition
forebrain development
adult behavior
maintenance of location
establishment of protein localization to organelle
response to metal ion
response to xenobiotic stimulus
tissue migration
cytokinesis
regeneration
response to alcohol
embryonic organ development
lipid modification
ribonucleoprotein complex biogenesis
microvillus organization
peptidyl-serine modification
carbohydrate biosynthetic process
negative regulation of protein localization
negative regulation of protein modification process
-2.5 -2.0 -1.5 -1.0 -0.5 0.0 0.5 1.0 1.5 2.0 2.5
Normalized Enrichment Score
control #2 versus patient #2 (KEGG-Pathway)
Proteoglycans in cancer
Herpes simplex virus 1 infection
Motor proteins
Adrenergic signaling in cardiomyocytes
Focal adhesion
Huntington disease
Autophagy
Pathways of neurodegeneration
Cell adhesion molecules
cGMP-PKG signaling pathway
Pathways in cancer
Bacterial invasion of epithelial cells
Axon guidance
Insulin signaling pathway
MAPK signaling pathway
Amyotrophic lateral sclerosis
Tight junction
-1.0 -0.5 0.0 0.5 1.0 1.5 2.0 2.5
Normalized Enrichment Score
c
control #2 versus patient #3 (GO-BP)
neuron cellular homeostasis
microtubule polymerization or depolymerization
regulation of blood circulation
regulation of neuron projection development
potassium ion transport
regulation of developmental growth
positive regulation of cell projection organization
regulation of microtubule-based process
microtubule bundle formation
heart process
regeneration
meiotic cell cycle
sensory system development
respiratory tube development
respiratory system development
protein polyubiquitination
mitochondrion localization
hindbrain development
regulation of membrane permeability
appendage development
-2.0 -1.5 -1.0 -0.5 0.0 0.5 1.0 1.5 2.0 2.5
Normalized Enrichment Score
control #2 versus patient #3 (KEGG-Pathway)
Lysosome
Huntington disease
Endocytosis
GABAergic synapse
Epithelial cell signaling in Helicobacter pylori infection
Cardiac muscle contraction
Alzheimer disease
Motor proteins
Salmonella infection
Pathways of neurodegeneration
Long-term potentiation
Amphetamine addiction
HIF-1 signaling pathway
Thermogenesis
Transcriptional misregulation in cancer
Apelin signaling pathway
Relaxin signaling pathway
Ubiquitin mediated proteolysis
PI3K-Akt signaling pathway
Alcoholism
-2.5 -2.0 -1.5 -1.0 -0.5 0.0 0.5 1.0 1.5 2.0 2.5
Normalized Enrichment Score
d
control #4 versus patient #4 (GO-BP)
regulation of membrane potential
microtubule polymerization or depolymerization
regulation of monoatomic ion transport
regulation of transmembrane transport
Golgi organization
regulation of kinase activity
positive regulation of MAPK cascade
muscle cell proliferation
regulation of microtubule-based process
muscle system process
proteasome-mediated ubiquitin-dependent protein catabolic process
smoothened signaling pathway
organic acid transport
regulation of mRNA metabolic process
hindbrain development
protein localization to cilium
nucleotide-excision repair
viral process
fatty acid metabolic process
protein polyubiquitination
-2.5 -2.0 -1.5 -1.0 -0.5 0.0 0.5 1.0 1.5 2.0 2.5
Normalized Enrichment Score
control #4 versus patient #4 (KEGG-Pathway)
cGMP-PKG signaling pathway
Cardiac muscle contraction
MAPK signaling pathway
Alzheimer disease
Oxytocin signaling pathway
Hypertrophic cardiomyopathy
Dilated cardiomyopathy
Adrenergic signaling in cardiomyocytes
Human cytomegalovirus infection
Renin secretion
Necroptosis
Pancreatic cancer
Insulin resistance
HIF-1 signaling pathway
Ubiquitin mediated proteolysis
-2.0 -1.5 -1.0 -0.5 0.0 0.5 1.0 1.5 2.0 2.5
Normalized Enrichment Score

Figure S3

a

b

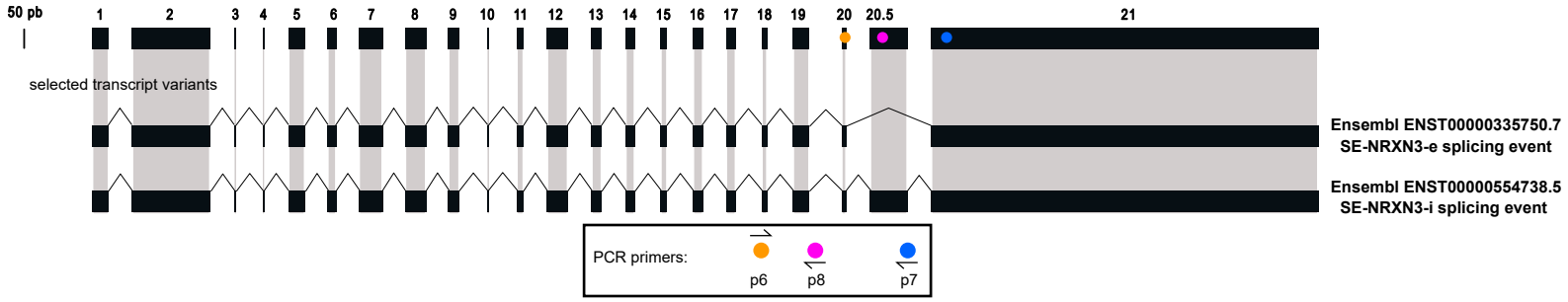

c

primer combination	intended target transcript	example sequence	frequency in control	frequency in PTHS
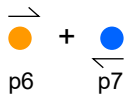	**SE-NRXN3-e splicing variant** 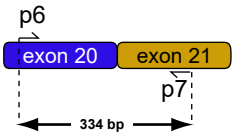	AAGTGATGATGAAGACTTTGTTGAATGTGA GCCGAGTACAGATAAGAGTCTTTCCACTTC AATCTTCGAAGGTGGCTACAAAGCACATGC GCCCAAGTGGGAATCCAAGGACTTTAGACC TAACAAAGTCTCCGAAACTAGTAGGACTAC TACCACATCTTTATCCCCTGAGCTGATCCG CTTCACAGCTTCCTCCTCGTCTGGGATGGT GCCCAAATTGCCAGCTGGCAAAATGAATAA CCGTGATCTCAAACCCCAGCCTGATATAGT CTTGCTTCCGTTGCCCACTGCCTATGA	14 (19)	15 (17)
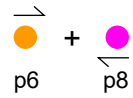	**SE-NRXN3-i splicing variant** 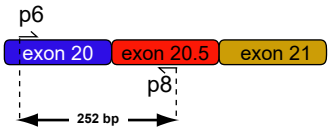	TGAATGTGAGCCGAGTACAGGTAGGTCAGC CAGAAGCTCTAATGCAGCTAGATCACTCCG TGCCGCCCTTACATGGACATGGCGACTCAC TTACACATTTACTCCTATCATCTTCATCTC CTGTGTAGTTCACTCATAGATATGACCCTC CCCTTCCTGCATCTTTCCTTCCCATTCTCC CCCTTTCTTTAGCATTGTTAAAATTTATGT GCTGTCATCCATCTCCAATCACTAG	2 (19)	0 (17)